# A Dynamics Based Method for Accelerometer-Only Navigation of a Spinning Projectile

by

Paul James Goulart

S.B. Aeronautics and Astronautics,
Massachusetts Institute of Technology, 1998

Submitted to the Department of Aeronautics and Astronautics
in partial fulfillment of the requirements for the degree of

Master of Science in Aeronautics and Astronautics

at the

MASSACHUSETTS INSTITUTE OF TECHNOLOGY

September 2001



Author .....
Department of Aeronautics and Astronautics
September 1, 2001

Certified by .....
Dr. Matthew Bottkol
Technical Staff, Charles Stark Draper Laboratory
Thesis Supervisor

Certified by .....
Prof. Steven R. Hall
Professor of Aeronautics and Astronautics
Thesis Supervisor

Accepted by .....
Prof. Wallace E. Vander Velde
Professor of Aeronautics and Astronautics
Chair, Committee on Graduate Students

# A Dynamics Based Method for Accelerometer-Only Navigation of a Spinning Projectile

by

Paul James Goulart

Submitted to the Department of Aeronautics and Astronautics
on September 1, 2001, in partial fulfillment of the
requirements for the degree of
Master of Science in Aeronautics and Astronautics

## Abstract

A method of navigating a gun-launched, spinning projectile using only accelerometers is presented. A linear combination of the outputs of a general configuration of at least 12 accelerometers is shown to provide measurements of angular acceleration and angular rate products of the form $\omega_i^2$ and $\omega_i\omega_j$. These measurements are used in the development of a 12 state, extended Kalman filter to estimate position, velocity, attitude, and angular rate, with twelve additional states included to estimate accelerometer biases.

Assumptions about the dynamic behavior of the vehicle are used to assist in attitude estimation. These assumptions come in two parts. First, that the nose of the vehicle remains pointed along the air-relative velocity vector during flight. Second, that the vehicle lateral angular rates have a secular component due to the vehicle pitching over during flight to maintain this alignment. A digital filter is used to isolate the secular pitch-over component of the estimated rate in an intermediate, non-rolling frame. These dynamics-based estimates are then incorporated as measurements in the navigation filter.

A configuration of 12 accelerometers arranged on the faces of a 10 cm cube is used in a six degree of freedom simulation to navigate a projectile spinning at 2 Hz. The navigation filter is shown to reliably estimate angular rates with biases as large as 1 g. Bias state estimation is also shown to compensate for instrument misalignments up to 1 degree. Using the dynamics-based measurements, the navigation filter successfully estimates projectile roll attitude to within 20 degrees for instrument random walk errors up to 2.5 milli-g/$\sqrt{\text{Hz}}$.

Thesis Supervisor: Dr. Matthew Bottkol
Title: Technical Staff, Charles Stark Draper Laboratory

Thesis Supervisor: Prof. Steven R. Hall
Title: Professor of Aeronautics and Astronautics

# Acknowledgments

I would like to thank all of the people who have helped and supported me during the writing of this thesis, and during my time at MIT.

Thanks to the many Draper staff who I have had the opportunity of working with over the last two years: Chris D'Souza, Chris Stoll, Time Brand, Don Gustafson, George Schmidt, Tom Thorvaldsen, and Dave Geller. Special thanks to Dave for letting me borrow the same book so many times.

Thanks very much to my thesis supervisor at Draper, Matt Bottkol, for his time, advice, and encouragement, and for helping me to find a good topic. Thanks also to my thesis advisor, Prof. Steven Hall, for his many helpful suggestions, comments, and clarifications.

Thanks to the many other Draper Fellows who I've spent the last two years with: Andre Girerd, John Stedl, Andrew Grubler, and Raja Chari. Thanks especially to Jeremy Rea for studying for the quals with me. Many thanks also to all of the friends I have made in Cambridge and at MIT over the last few years.

Thanks to my family for their continuing love, support, and encouragement.

Finally, thanks to my fiancée Emma for her love, patience, and sacrifice.

ACKNOWLEDGMENT
08/01/01

This thesis was prepared at The Charles Stark Draper Laboratory, Inc., under NAVSEA PMS529 Contract N00024-01-C-5247.
Publication of this thesis does not constitute approval by Draper or the sponsoring agency of the findings or conclusions contained herein. It is published for the exchange and stimulation of ideas.
Permission is hereby granted by the author to the Massachusetts Institute of Technology to reproduce any ar all of this thesis.

Paul J. Goulart

# Contents

# List of Figures

# List of Tables

## Symbols

| | |
|---|---|
| $\mathbf{A}_{IB}$ | $3 \times 3$ body to inertial frame transformation matrix |
| $\boldsymbol{a}_i$ | total acceleration of $i$th accelerometer |
| $\mathbf{E}$ | pseudo-inverse of accelerometer transformation matrix. $\mathbf{E} = \mathbf{M}^{\#}$ |
| $\mathbf{F}$ | state transformation matrix (continuous time) |
| $\boldsymbol{f}_i$ | output of $i$th accelerometer |
| $\boldsymbol{g}$ | gravity vector |
| $\mathbf{C}$ | matrix of measurement partial derivatives |
| $\mathbf{I}$ | identity matrix or $3 \times 3$ inertia tensor |
| $\mathbf{I}_r$ | roll component isolation matrix. $\mathbf{I}_r = \text{diag}\left(\begin{bmatrix} 1 & 0 & 0 \end{bmatrix}\right)$ |
| $\mathbf{I}_t$ | transverse component isolation matrix. $\mathbf{I}_t = \text{diag}\left(\begin{bmatrix} 0 & 1 & 1 \end{bmatrix}\right)$ |
| $\mathbf{K}$ | Kalman gain matrix |
| $\mathbf{M}$ | accelerometer transformation matrix. $\boldsymbol{\eta} = \mathbf{M}\boldsymbol{f}$ |
| $\mathbf{P}$ | covariance matrix |
| $\mathbf{Q}$ | process noise matrix |
| $\boldsymbol{q}$ | inertial to body frame attitude quaternion. $\boldsymbol{q} = [\boldsymbol{q}_v, q_s]$ |
| $\mathbf{R}$ | measurement noise matrix |
| $\boldsymbol{r}_I$ | projectile position (inertial frame) |
| $\boldsymbol{r}_i$ | body frame position of $i$th accelerometer |
| $\boldsymbol{s}_B$ | linear acceleration at origin of body reference frame |
| $\boldsymbol{v}_B$ | projectile velocity (body frame) |
| $\boldsymbol{v}_I$ | projectile velocity (inertial frame) |
| $\mathbf{W}$ | matrix of angular rate products $[\boldsymbol{\omega}\times][\boldsymbol{\omega}\times]$ |
| $\boldsymbol{w}_s$ | vector of rate square terms, i.e. $\omega_x^2$ |
| $\boldsymbol{w}_c$ | vector of rate cross terms, i.e. $\omega_x\omega_y$ |
| $\boldsymbol{z}$ | measurement for Kalman filter |

$\boldsymbol{\alpha}_B$ angular acceleration in body frame

$\boldsymbol{\beta}$ vector of accelerometer biases

$\gamma$ vehicle flight path angle

$\boldsymbol{\eta}$ vector of vehicle accelerations and rate products

$\boldsymbol{\theta}_i$ body frame orientation of $i$th accelerometer

$\boldsymbol{\lambda}_i$ misalignment vector for $i$th accelerometer

$\boldsymbol{\nu}$ white noise process

$\sigma_{rw}$ accelerometer random walk error

$\boldsymbol{\Phi}$ state transformation matrix (discrete time)

$\boldsymbol{\psi}$ attitude perturbation state

$\boldsymbol{\omega}_B$ angular rate in body frame

## Notation

$x$ scalar quantity

$\mathbf{X}$ matrix quantity

$\boldsymbol{x}$ vector quantity

$\hat{\boldsymbol{x}}$ estimated value of $\boldsymbol{x}$

$\bar{\boldsymbol{x}}$ nominal or reference value of $\boldsymbol{x}$

$\mathrm{tr}(\mathbf{X})$ trace of matrix $\mathbf{X}$

E[x] expected value of x

$[\boldsymbol{x}\times]$ matrix form of the cross product. $[\boldsymbol{x}\times] = \begin{bmatrix} 0 & -x_z & x_y \\ x_z & 0 & -x_x \\ -x_y & x_x & 0 \end{bmatrix}$

# Chapter 1

# Introduction

## 1.1 Background

For several years, munitions research programs underway at Draper Laboratory such as the Extended Range Guided Munitions Demonstration (ERGM Demo) [4], and the Competent Munition Advanced Technology Demonstration (CMATD), have sought to develop low cost guidance and navigation systems for spin-stabilized, gun-launched projectiles. The environments in which these systems must operate present several unique challenges for inertial navigation.

During the boost phase, gun-launched systems can experience shocks in excess of 10,000 g, which can cause significant changes to instrument alignment, bias, scale factors, etc., requiring significant in-flight instrument calibration [5]. On the ERGM system, the guidance and control system requires that the navigation system be capable of providing an initial estimate of local vertical (termed *down determination*) to within approximately 15-20 degrees, without the benefit of any kind of external measurement such as GPS. Systems such as ERGM solve this problem by noting that the lateral rates of the projectile must have a component attributable to the slow pitching over of the vehicle as it seeks to remain aligned with the flight path [6, 8].

Typically, inertial navigation systems rely on a combination of high quality inertial instrumentation and precise knowledge of initial conditions for attitude determination. In these systems, no models of the vehicle dynamics are required, since the uncertainty in the models greatly exceeds the uncertainty in initial conditions and instrument calibration.

A gun-launched projectile suffers from very poor knowledge of initial conditions, particulary initial roll attitude. The very high g forces experienced during launch prevent measurement integration during the firing phase, due to instrument saturation. While the initial vehicle pointing direction can be assumed to be approximately aligned with the firing direction during filter initialization, the roll orientation is likely to be completely unknown. Unlike a standard inertial navigation system, whose instruments can be very finely calibrated prior to launch, a gun-launched system must do a substantial amount of instrument calibration in-flight.

The solution to the problems of in-flight state estimation and instrument calibration is to exploit the known dynamics of the vehicle to make corrections to the vehicle

state. This is achieved through formulation of *pseudo-measurements*: information about the state that is not actually measured, but rather is assumed based on vehicle properties and presented to the navigation algorithm as a real measurement.

An effort is also under way at Draper to develop a Low Cost Guidance Electronics Unit (LCGEU) using Commercial-Off-The-Shelf (COTS) accelerometers exclusively [9], in place of the more costly and less robust accelerometer/gyro package used in previous munitions. Replacement of the three gyros with three additional accelerometers allows the accelerometer package to take on the dual roll of measuring both linear and angular acceleration, which can be integrated to obtain the angular rate.

An additional six accelerometers provide further information about the angular rate, but in the form of non-linear rate products of the form $\omega_x^2$ and $\omega_x\omega_y$ resulting from centripetal acceleration. These measurements can be used to help stabilize integration of the angular acceleration.

The means by which angular rate is estimated requires another departure from ordinary inertial navigation techniques. Typically, gyros in a navigation system provide a direct measurement of the angular rate. In the accelerometer-only case, only angular accelerations can be measured directly, requiring the angular rate to be added to the navigation algorithm explicitly as a filter state.

## 1.2 Thesis Objectives and Overview

This thesis seeks to develop an navigation solution for a gun-launched projectile. An integrated navigation filter predicated on work by Asher [1] is proposed to estimate position, velocity, attitude, and angular rate using only accelerometers and, when available, GPS. By itself, this algorithm provides estimates of angular rate, but is not capable of accurately estimating vehicle orientation, especially when no initial attitude estimate is available.

It is still possible, however, to estimate vehicle orientation by noting that a projectile tends to pitch over during flight to align itself with its wind-relative velocity vector. Roll orientation can then found by isolating this component of the lateral angular rate, and assuming that it is aligned with a vector normal to the projectile flight path.

A new technique for sensing this pitch-over component is developed, as well as a method of incorporating this and other dynamics-based information into the integrated navigation framework. Filter performance is then used to estimate upper bounds on the accelerometer performance required to achieve the stated project goal of 20 deg roll attitude estimation accuracy.

The present chapter gives an overview of the problem and the motivation for its solution. It also briefly covers related work in accelerometer-only navigation, and the difficulties of navigating a spinning projectile without use of external reference.

Chapter 2 describes the 6-DOF environment developed for simulation, and presents the dynamical, atmospheric, and aerodynamic models employed in the simulation.

Chapter 3 derives the relationship between the motion of a general rotating body and the outputs of accelerometers fixed to the rotating frame of reference. These

equations are inverted to show how, given twelve independently oriented instruments, the angular acceleration, specific force, and six different rate products can be measured. A direct solution of the angular rates is developed for the special case of a body spinning about a primary axis with error-free instruments. The nominal sensor configuration used in subsequent sections is also presented.

Chapter 4 develops a Kalman filter solution to the basic navigation problem. First, appropriate navigation states are defined for 6-DOF navigation, and linearized state transition equations are derived for the special case of accelerometer-only navigation. Measurement equations are derived for the accelerometer outputs, as well as for external reference data from GPS position and velocity measurements. Simple formulas for state propagation and error correction are presented.

Chapter 5 extends the basic navigation algorithm to include predictions regarding the behavior of the projectile during flight. These predictions come in two parts: first, that the nose of the vehicle should remain pointed along the air-relative velocity vector during flight; and second, that the vehicle lateral rates should have a secular component consistent with the expected gravity turn rate, or pitch-over rate. A method of separating the pitch-over component of the lateral rate from the higher frequency precession and nutation components using a simple IIR digital filter is proposed. These predictions are then formulated as pseudo-measurements, and incorporated into the original navigation algorithm.

Chapter 6 presents simulation results for rate attitude estimation. The effects of each of the major sources of instrument error on rate estimation are investigated. IIR filter parameterization and performance are discussed in the context of the pitch-over measurement. Angular rate and roll attitude estimation performance is examined for increasing levels of instrument error.

Chapter 7 summarizes the performance of the proposed navigation algorithm. Conclusions are drawn about the feasibility of accelerometer-only navigation, and suggestions for future research are made.

# Chapter 2

# Simulation Environment

In order to provide a realistic testing environment for the navigation methods developed in this thesis, a 6-DOF simulation environment was created using Simulink, with navigation algorithms implemented in Matlab. A top level view of the simulation environment is shown in Figure 2-1. Vehicle parameters for the simulation are based on a generic gun-launched projectile model developed at Draper Laboratory[2]. Section 2.1 describes the equations of motion used in the simulation, Section 2.2 describes the atmospheric model, and Section 2.3 describes modelling of the aerodynamic forces on the vehicle.

## 2.1 Equations of Motion

The vehicle position, velocity, attitude, and angular rate are modelled in a 6-DOF simulation in Simulink using a flat earth gravitational model. The translational equation of motion is

$$\ddot{\boldsymbol{x}}_I = \boldsymbol{g}_I + Lift + Drag \tag{2.1}$$

The rotational equation of motion is

$$\mathbf{I}\dot{\boldsymbol{\omega}}_B = Moment + \boldsymbol{\omega}_B \times \mathbf{I}\boldsymbol{\omega}_B \tag{2.2}$$

where lift, drag, and moment are vector valued quantities in the appropriate frames.

Vehicle orientation is represented by an attitude quaternion in simulation, which is propagated using

$$\dot{\boldsymbol{q}} = \frac{1}{2}\begin{bmatrix} 0 & \omega_z & -\omega_y & \omega_x \\ -\omega_z & 0 & \omega_x & \omega_y \\ \omega_y & -\omega_x & 0 & \omega_z \\ -\omega_x & -\omega_y & -\omega_z & 0 \end{bmatrix} \boldsymbol{q} \tag{2.3}$$

where the scalar component of $\boldsymbol{q}$ is in the last term.

Physical property values for the projectile model, plus nominal launch conditions, are provided in Tables 2.1 and 2.2. An example of a typical vehicle trajectory is shown in Figure 2-2.

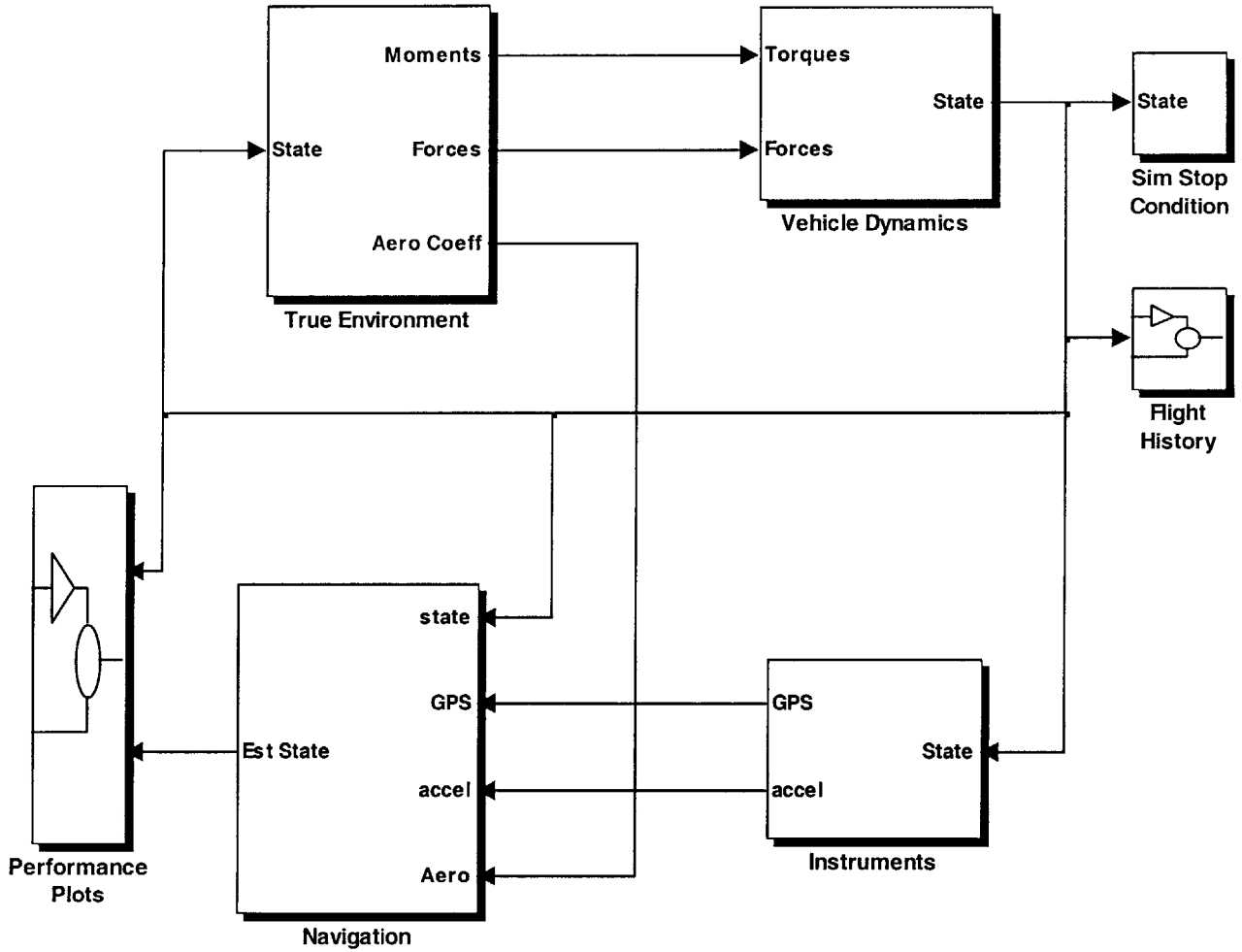


Figure 2-1: View of Simulation Environment

Table 2.1: Nominal launch conditions

| | |
|---|---|
| Launch Elevation | 45 deg |
| Launch Velocity | 550 m/s |
| Roll Rate ($\omega_x$) | 2 Hz |

Table 2.2: Vehicle properties

| | |
|---|---|
| Mass (m) | 30 kg |
| Moment of Inertia ($I_X$) | 0.054 kg $\cdot$ m$^2$ |
| Moment of Inertia ($I_T$) | 0.252 kg $\cdot$ m$^2$ |
| Radius | 0.06 m |
| Length | 0.3 m |

## 2.2 Atmospheric Model

The atmospheric density used to calculate aerodynamic forces on the vehicle body is approximated by a simple adiabatic model of the atmosphere. While this method is less accurate than using tabulated atmospheric data, it has the advantage of running significantly faster than a table lookup when implemented in the Simulink environment, and does not vary markedly from tabular data at the altitudes involved. Assumed atmospheric conditions at sea level are shown in Table 2.3.

The temperature at altitude $h$ is

$$\frac{T}{T_0} = 1 - \frac{\gamma}{\gamma - 1}\frac{gh}{RT_0} \tag{2.4}$$

where $T_0$ is the surface air temperature. The air pressure at altitude $h$ is

$$\frac{P}{P_0} = \left[1 - \frac{\gamma}{\gamma - 1}\frac{gh}{RT_0}\right]^{\frac{\gamma}{\gamma-1}} \tag{2.5}$$

where $P_0$ is the surface pressure. The air density is then just

$$\rho = \frac{P}{RT} \tag{2.6}$$

or

$$\rho = \frac{P_0}{RT_0}\left[1 - \frac{\gamma}{\gamma - 1}\frac{gh}{RT_0}\right]^{\frac{1}{\gamma-1}} \tag{2.7}$$

## 2.3 Aerodynamic Forces

Aerodynamic coefficients are based on a generic projectile model developed at Draper. Lift, drag, and pitching coefficients are modelled as functions of Mach number ($M$) and angle of attack ($\alpha$) in degrees. These values are included as Table 2.4.

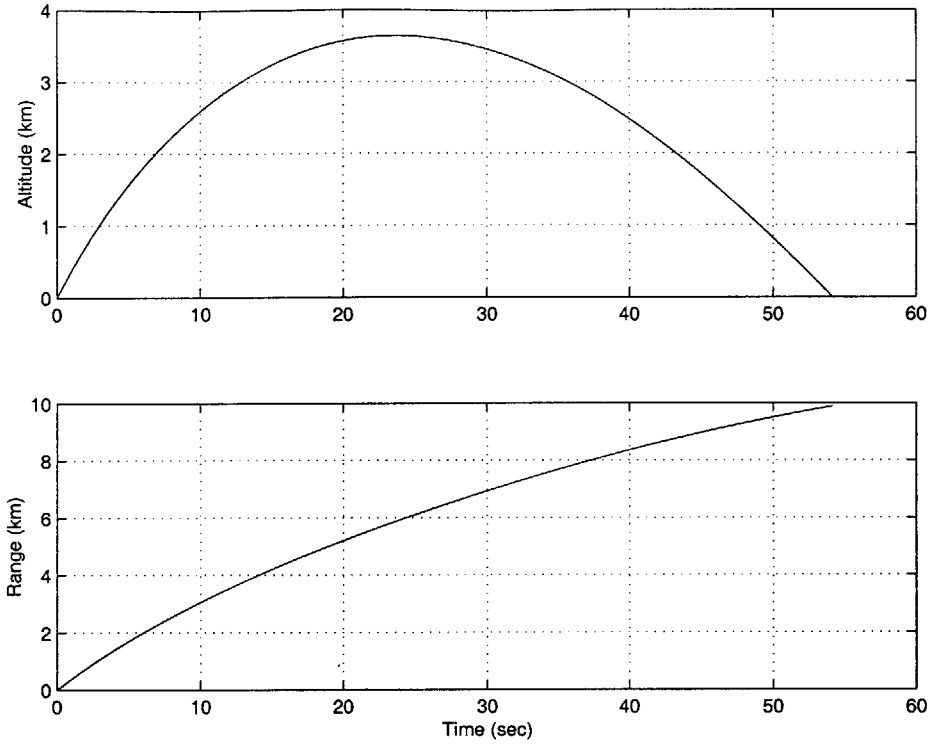


Figure 2-2: Typical vehicle trajectory

Table 2.3: Atmospheric conditions

| | |
|---|---|
| Surface Air Temperature ($T_0$) | 298.16 K |
| Surface Air Pressure ($P_0$) | 1.013e5 N/m$^2$ |
| Gas Constant (R) | 287 J/kg/K |
| Specific Heat Ratio ($\gamma$) | 1.4 |

The dynamic pressure can be defined as

$$q_\infty = \frac{1}{2}\rho |\boldsymbol{v}|^2 \tag{2.8}$$

where $\rho$ is the atmospheric density found in 2.6. Taking velocities in the body frame, the transverse component of velocity can be written as

$$\boldsymbol{v}_t = \begin{bmatrix} 0 & v_{B_y} & v_{B_z} \end{bmatrix}^T \tag{2.9}$$

and the angle of attack defined as

$$\alpha = \sin^{-1}\left(\frac{|\boldsymbol{v}_t|}{|\boldsymbol{v}_B|}\right) \tag{2.10}$$

Table 2.4: Aerodynamic coefficients

| | |
|---|---|
| Reference Area ($A_{\text{ref}}$) | 0.0113 $\text{m}^2$ |
| Reference Length ($L_{\text{ref}}$) | 0.3 m |
| $C_{m_\alpha}$ | $-0.028290\ M\alpha$ |
| | $-0.00196\ M$ |
| | $+0.16126\ \alpha$ |
| | $+0.00127$ |
| $C_{d_0}$ | $0\ M\alpha$ |
| | $0\ M$ |
| | $-0.13650\ \alpha$ |
| | $+0.74235$ |
| $C_{d_\alpha}$ | 0 |

Defining the additional unit vectors

$$\boldsymbol{i}_n = -\frac{\boldsymbol{v}_t}{|\boldsymbol{v}_t|} \tag{2.11}$$

$$\boldsymbol{i}_m = \frac{[\ 0 \quad +i_{n_z} \quad -i_{n_y}\ ]^{\mathrm{T}}}{\left|[\ 0 \quad +i_{n_z} \quad -i_{n_y}\ ]^{\mathrm{T}}\right|} \tag{2.12}$$

$$\boldsymbol{i}_x = [\ 1 \quad 0 \quad 0\ ]^T \tag{2.13}$$

the moment, lift force, and drag force of 2.1 and 2.1 can be defined as

$$\mathit{Lift} = A_{\text{ref}} C_{m_\alpha} \alpha q_\infty \boldsymbol{i}_n \tag{2.14}$$

$$\mathit{Drag} = -A_{\text{ref}} \left(C_{d_0} + C_{d_\alpha} \alpha^2\right) q_\infty \boldsymbol{i}_x \tag{2.15}$$

$$\mathit{Moment} = A_{\text{ref}} L_{\text{ref}} C_{m_\alpha} \alpha q_\infty \boldsymbol{i}_m \tag{2.16}$$

# Chapter 3

# Measurement Transformations

As discussed in Chapter 1, the elimination of gyros in the navigation system of a gun-launched projectile would have significant advantages in terms of cost and launch reliability. In order for gyro-free navigation to succeed, a method of estimating angular rates using only accelerometer outputs must be developed. This is possible in a spinning projectile because the outputs of the accelerometers will have components due to both centripetal and Euler accelerations in the body-fixed reference frame.

This chapter defines the relationships between the motion of a general rotating body and the outputs of accelerometers fixed to the rotating frame of reference. Section 3.1 is based on previous work by Asher [1], and derives the relationships between vehicle state and accelerometer outputs, and shows them to be linear functions of the vehicle linear acceleration, angular acceleration, and rate products of the form $\omega_i^2$ and $\omega_i\omega_j$. Section 3.2 describes a deterministic method of recovering the angular rate from the accelerometer outputs in the case of error-free sensors. This method is greatly improved upon by the Kalman filtering method to be presented in Chapter 4. Finally, Section 3.3 presents the nominal configuration of 12 accelerometers used throughout the remainder of the thesis.

## 3.1 Accelerometer Outputs

The acceleration of a point $\boldsymbol{r}_i$ within a rotating reference frame is

$$\boldsymbol{a}_i = \boldsymbol{s}_B + \boldsymbol{\alpha}_B \times \boldsymbol{r}_i + \boldsymbol{\omega}_B \times \boldsymbol{\omega}_B \times \boldsymbol{r}_i \tag{3.1}$$

where $\boldsymbol{s}_B$ is the acceleration resulting from the body specific force vector at the origin of the coordinate system, $\boldsymbol{\alpha}_B$ is the angular acceleration, and $\boldsymbol{\omega}_B$ is the angular rate. The output of an accelerometer at this point with sensitive axis aligned along the unit orientation vector $\boldsymbol{\theta}_i$ relative to the body frame is[1]

$$f_i = \boldsymbol{s}_B \cdot \boldsymbol{\theta}_i + [\boldsymbol{\alpha}_B \times \boldsymbol{r}_i] \cdot \boldsymbol{\theta}_i + ([\boldsymbol{\omega}_B\times]\,[\boldsymbol{\omega}_B\times]\,\boldsymbol{r}_i) \cdot \boldsymbol{\theta}_i \tag{3.2}$$

[1]The matrix form of the cross product is used throughout. Expressions such as $[\boldsymbol{a}\times]$ are equivalent to the $3 \times 3$ matrix of vector components $\begin{bmatrix} 0 & -a_z & a_y \\ a_z & 0 & -a_x \\ -a_y & a_x & 0 \end{bmatrix}$. The expressions $\boldsymbol{a} \times \boldsymbol{b}$ and $[\boldsymbol{a}\times]\boldsymbol{b}$ are equivalent.

The final term in (3.2) contains the centripetal acceleration, which can alternatively be written in matrix form as

$$[\boldsymbol{\omega}_B\times]\,[\boldsymbol{\omega}_B\times] = \begin{bmatrix} -\omega_y^2-\omega_z^2 & \omega_y\omega_x & \omega_z\omega_x \\ \omega_x\omega_y & -\omega_x^2-\omega_z^2 & \omega_z\omega_y \\ \omega_x\omega_z & \omega_y\omega_z & -\omega_x^2-\omega_y^2 \end{bmatrix} \tag{3.3}$$

This gives six different rate products, representing both square and cross product terms. These terms can be represented by a symmetric matrix $\mathbf{W}$ of rate products, so that (3.3) can be rewritten as

$$[\boldsymbol{\omega}_B\times]\,[\boldsymbol{\omega}_B\times] = \begin{bmatrix} W_{11} & W_{12} & W_{13} \\ W_{12} & W_{22} & W_{23} \\ W_{13} & W_{23} & W_{33} \end{bmatrix} \tag{3.4}$$

Using this expression for $\mathbf{W}$, and rewriting (3.2) in matrix form gives

$$f_i = \boldsymbol{\theta}_i^{\mathrm{T}}\boldsymbol{s}_B - \boldsymbol{\theta}_i^{\mathrm{T}}[\boldsymbol{r}_i\times]\,\boldsymbol{\alpha}_B + \boldsymbol{r}_i^{\mathrm{T}}\mathbf{W}\boldsymbol{\theta}_i \tag{3.5}$$

Ideally, the output of the $i$th accelerometer should be written as a linear combination of the angular acceleration and rate product terms. This can be done by recognizing that the final term in (3.5) can be rewritten to isolate the elements of $\mathbf{W}$, so that

$$\boldsymbol{r}_i^{\mathrm{T}}\mathbf{W}\boldsymbol{\theta}_i = \begin{bmatrix} \theta_{i_1}r_{i_2}+\theta_{i_2}r_{i_1} \\ \theta_{i_1}r_{i_3}+\theta_{i_3}r_{i_1} \\ \theta_{i_2}r_{i_3}+\theta_{i_3}r_{i_2} \\ \theta_{i_1}r_{i_1} \\ \theta_{i_2}r_{i_2} \\ \theta_{i_3}r_{i_3} \end{bmatrix}^{\mathrm{T}} \begin{bmatrix} W_{12} \\ W_{13} \\ W_{23} \\ W_{11} \\ W_{22} \\ W_{33} \end{bmatrix} = \begin{bmatrix} \boldsymbol{m}^{\mathrm{T}} & \boldsymbol{n}^{\mathrm{T}} \end{bmatrix} \begin{bmatrix} \boldsymbol{w}_c \\ \boldsymbol{w}_s \end{bmatrix} \tag{3.6}$$

where $\boldsymbol{w}_c$ represents the vector of cross term components of $\mathbf{W}$, and $\boldsymbol{w}_s$ represents the square terms. The full set of accelerometer outputs can then be expressed in matrix form as

$$\begin{bmatrix} f_1 \\ f_2 \\ \vdots \\ f_n \end{bmatrix} = \begin{bmatrix} \boldsymbol{\theta}_1^{\mathrm{T}} & -\boldsymbol{\theta}_1^{\mathrm{T}}\{\boldsymbol{r}_1\times\} & \boldsymbol{m}_1^{\mathrm{T}} & \boldsymbol{n}_1^{\mathrm{T}} \\ \boldsymbol{\theta}_1^{\mathrm{T}} & -\boldsymbol{\theta}_2^{\mathrm{T}}\{\boldsymbol{r}_2\times\} & \boldsymbol{m}_2^{\mathrm{T}} & \boldsymbol{n}_2^{\mathrm{T}} \\ \vdots & \vdots & \vdots & \vdots \\ \boldsymbol{\theta}_n^{\mathrm{T}} & -\boldsymbol{\theta}_n^{\mathrm{T}}\{\boldsymbol{r}_n\times\} & \boldsymbol{m}_n^{\mathrm{T}} & \boldsymbol{n}_n^{\mathrm{T}} \end{bmatrix} \begin{bmatrix} \boldsymbol{s}_B \\ \boldsymbol{\alpha}_B \\ \boldsymbol{w}_c \\ \boldsymbol{w}_s \end{bmatrix} \tag{3.7}$$

or more compactly as

$$\boldsymbol{f} = \mathrm{M}\boldsymbol{\eta} \tag{3.8}$$

Using a set of at least twelve accelerometers, and assuming no instrument biases or errors, the body forces, angular accelerations, and rate products $\mathbf{W}$ can be found directly by taking the pseudo-inverse of $\mathrm{M}$ in (3.8), giving

$$\boldsymbol{\eta} = \mathrm{M}^{\#}\boldsymbol{f} = \mathbf{E}\boldsymbol{f} \tag{3.9}$$

where the pseudo-inverse $\mathbf{M}^{\#}$ is used to allow for the case of more than 12 accelerometers. This gives the specific force, angular acceleration, and rate products as linear functions of the accelerometer outputs. Selected components of the vector $\boldsymbol{\eta}$ can then be calculated through appropriate partitioning of the matrix $\mathbf{E}$.

$$\boldsymbol{\eta} = \begin{bmatrix} \boldsymbol{s}_B \\ \boldsymbol{\alpha}_B \\ \boldsymbol{w}_c \\ \boldsymbol{w}_s \end{bmatrix} = \begin{bmatrix} \mathbf{E}_1 \\ \mathbf{E}_2 \\ \mathbf{E}_3 \\ \mathbf{E}_4 \end{bmatrix} \boldsymbol{f} \tag{3.10}$$

## 3.2 Deterministic Solution for Angular Rates

It is possible in principle to determine the angular rate components directly from the sensor outputs if the accelerometers are assumed to be error-free. One way of accomplishing this is to note that the vector triple product

$$[\boldsymbol{\omega}_B\times][\boldsymbol{\omega}_B\times]\boldsymbol{\omega}_B = \mathbf{W}\boldsymbol{\omega}_B \tag{3.11}$$

should always be zero, since it is the orthogonal projection of the rate vector $\boldsymbol{\omega}_B$ onto itself. Using the estimates for the rate products found in (3.9) to construct $\mathbf{W}$, the *direction* of the rate vector can be found by looking for an eigenvector with a corresponding eigenvalue of 0. The *magnitude* of the rate vector can also be found by evaluating the trace of $\mathbf{W}$, giving

$$\mathrm{tr}\,[\mathbf{W}] = -2\left[\omega_x^2 + \omega_y^2 + \omega_z^2\right] \tag{3.12}$$

$$|\boldsymbol{\omega}_B| = \frac{\pm\sqrt{-\mathrm{tr}\,[\mathbf{W}]}}{2} \tag{3.13}$$

The sign ambiguity in (3.13) can be resolved by recognizing that for a spinning projectile, the sign of the angular rate about the spin axis is known, e.g. $\omega_x > 0$. Using this fact, and assuming an eigenvector of the form

$$\boldsymbol{e} = \begin{bmatrix} 1 & e_y & e_z \end{bmatrix}^{\mathrm{T}} \tag{3.14}$$

The product $\mathbf{W}\boldsymbol{e}$ can be rewritten as

$$\begin{bmatrix} W_{12} & W_{13} \\ W_{22} & W_{23} \\ W_{23} & W_{33} \end{bmatrix} \begin{bmatrix} e_y \\ e_z \end{bmatrix} = \begin{bmatrix} -W_{11} \\ -W_{12} \\ -W_{13} \end{bmatrix} \tag{3.15}$$

Since the terms $W_{22}$ and $W_{33}$ contain $-\omega_x^2$, their product should always be positive. Taking the last two equations, the components of $\boldsymbol{e}$ can be found using

$$e_y = \frac{-W_{12}W_{33} + W_{13}W_{23}}{+W_{22}W_{33} - W_{13}W_{23}} \tag{3.16}$$

Table 3.1: Accelerometer configuration

| | Position | | | Orientation | | |
|---|---|---|---|---|---|---|
| Accel # | x | y | z | x | y | z |
| 1 | $+d$ | 0 | 0 | 0 | 0 | +1 |
| 2 | $+d$ | 0 | 0 | 0 | +1 | 0 |
| 3 | $-d$ | 0 | 0 | 0 | +1 | 0 |
| 4 | 0 | $+d$ | 0 | +1 | 0 | 0 |
| 5 | 0 | $+d$ | 0 | 0 | 0 | +1 |
| 6 | 0 | $-d$ | 0 | 0 | 0 | +1 |
| 7 | 0 | 0 | $+d$ | 0 | +1 | 0 |
| 8 | 0 | 0 | $+d$ | +1 | 0 | 0 |
| 9 | 0 | 0 | $-d$ | +1 | 0 | 0 |
| 10 | $-d$ | 0 | 0 | +1 | 0 | 0 |
| 11 | 0 | $-d$ | 0 | 0 | +1 | 0 |
| 12 | 0 | 0 | $-d$ | 0 | 0 | +1 |

$$e_z = \frac{-W_{13}W_{22} + W_{12}W_{23}}{+W_{22}W_{33} - W_{13}W_{23}} \tag{3.17}$$

The rate vector is then

$$\boldsymbol{\omega}_B = \frac{\pm\sqrt{-\mathrm{tr}\,[\mathbf{W}]}}{2}\frac{\boldsymbol{e}}{|\boldsymbol{e}|} \tag{3.18}$$

with the sign determined by comparison to the known spin direction of the vehicle.

An alternate method of resolving the sign ambiguity in (3.18) is to make use of the angular acceleration information in $\mathbf{E}_2\boldsymbol{f}$. Comparison of rate estimates between successive updates with the angular acceleration would allow sign determination, but special care would need to be taken to properly account for sensor noise.

In practice, a deterministic solution for the rates is not practical, given the large biases and noise levels expected. Chapter 4 introduces a better Kalman filter based method of solving for rates in a noisy environment.

## 3.3 Instrument Configuration

For all subsequent work, the 12 instrument configuration proposed in [1] is used. This configuration places the instruments in orthogonal pairs on the faces of a cube, with one instrument from each pair of opposing sides facing radially outward from the center. A diagram of this arrangement is presented in figure (3-1). All instruments are equidistant from the cube center, with nominal displacement $d = 5$ cm. Table (3.1) gives the position and orientation of each sensor.

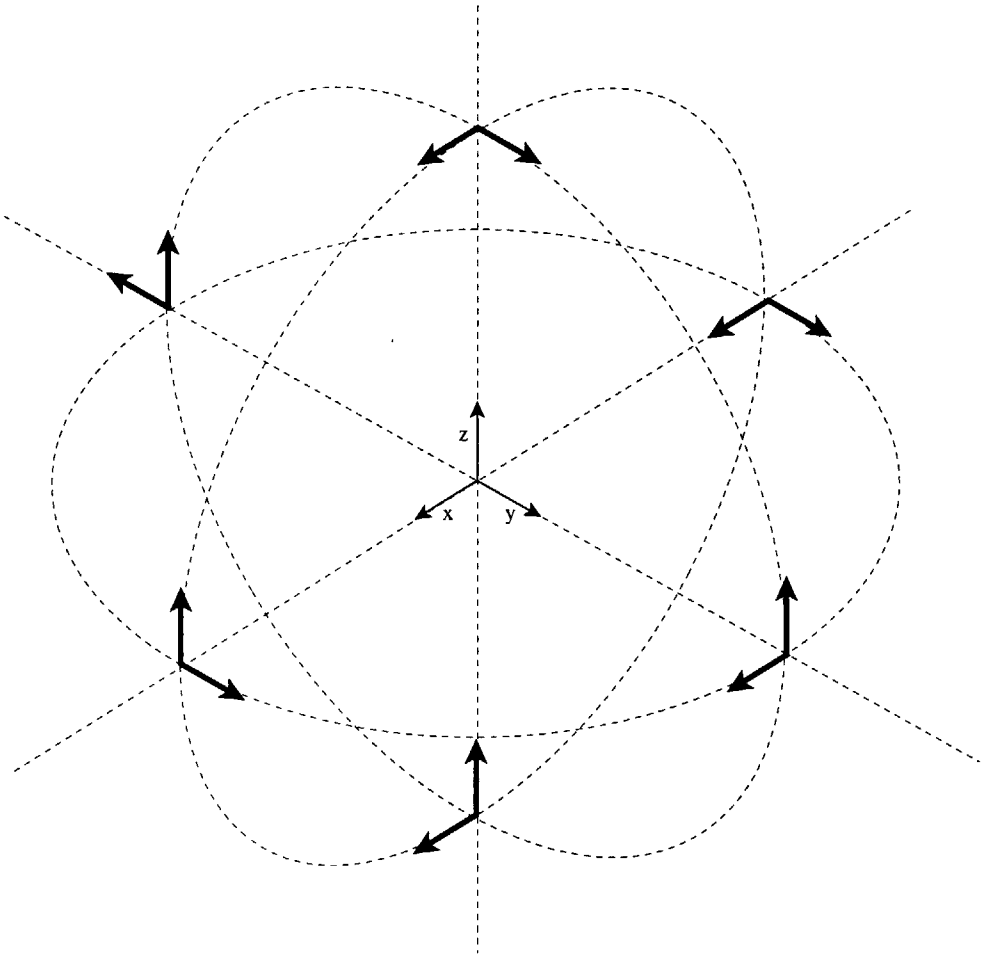


Figure 3-1: Accelerometer configuration

# Chapter 4

# Filter Implementation

Chapter 3 showed that an accelerometer-only navigation system can provide measurements of angular acceleration, which can then be integrated to provide an estimate of the angular rate. Linear combinations of the accelerometer outputs were also shown to provide measurements of angular rate products of the form $\omega_i^2$ and $\omega_i\omega_j$. It would be useful to develop a navigation filter that could use these additional measurements to help stabilize the integration of the angular rate, as well as to incorporate GPS measurements as they become available.

This chapter develops the 24-state Kalman filter used throughout the thesis. The filter includes 3 element states for perturbations in position, velocity, orientation, and angular rate, as well as 12 states for the accelerometer biases.

Section 4.1 presents the standard set of Kalman filter equations required by the navigation algorithm. Section 4.2 derives the linearized state equations used in the filter. The angular rate is included in this section as a state, since no direct measurement is available. The section concludes with a brief discussion of the possibility of accounting for sensor misalignments through bias estimation.

Section 4.3 describes how GPS measurements and measurements of the angular rate products $\omega_i^2$ and $\omega_i\omega_j$ are handled by the navigation filter. Since rate products are non-linear functions of the rate, measurement partials calculated in this section require the use of an extended Kalman filter. Position and velocity estimates from a pre-computed firing solution may provide a substitute in the absence of GPS prior to signal acquisition.

Section 4.4 describes how navigation system states are propagated and updated based on perturbation states calculated in the Kalman filter. While the attitude perturbation state is represented as a vector in 4.2, the total attitude estimate is characterized here in quaternion form, giving a 13 element vector for the reference state.

Section 4.5 describes the pitfalls of using a linearized filter for rate estimation. Techniques for reducing some of the errors characteristic of an extended Kalman filter during initialization are suggested.

## 4.1 Kalman Filter Equations

The Kalman filter is a recursive estimation algorithm devised by R.E. Kalman in 1960 [7], a derivation of which can be found, for example, in [3]. Since a spinning projectile has non-linear equations of motion, an extended Kalman filter formulation is used, where the filter states represent small perturbations $\delta\boldsymbol{x}$ of the vehicle state about its nominal value $\bar{\boldsymbol{x}}$. After each Kalman filter measurement update, the filter states are applied as corrections to the reference state, and are then reset to zero.

Using the discrete form of the filter, a small perturbation $\delta\boldsymbol{x}$ about the nominal trajectory evolves according to the state transition equation

$$\delta\boldsymbol{x}_k = \boldsymbol{\Phi}_k \delta\boldsymbol{x}_{k-1} + \boldsymbol{w}_k \tag{4.1}$$

where $\boldsymbol{\Phi}$ is the state transition matrix, and $\boldsymbol{w}_k$ is a process noise term with covariance given by

$$\mathbf{Q}_k = \mathrm{E}[\boldsymbol{w}_\mathrm{k}\boldsymbol{w}_\mathrm{k}^\mathrm{T}] \tag{4.2}$$

Estimates of the state perturbation before and after the $k$th measurement is included are written as $\delta\hat{\boldsymbol{x}}_k^-$ and $\delta\hat{\boldsymbol{x}}_k^+$, respectively, and are updated between measurements using the state transition equation

$$\delta\hat{\boldsymbol{x}}_k^- = \boldsymbol{\Phi}_k \delta\hat{\boldsymbol{x}}_k^+ \tag{4.3}$$

The covariance of the estimation error is given by

$$\mathbf{P}_k = \mathrm{E}[(\delta\boldsymbol{x}_\mathrm{k} - \delta\hat{\boldsymbol{x}}_\mathrm{k})(\delta\boldsymbol{x}_\mathrm{k} - \delta\hat{\boldsymbol{x}}_\mathrm{k})^\mathrm{T}] \tag{4.4}$$

and is updated between time steps using the covariance transition equation

$$\mathbf{P}_k^- = \boldsymbol{\Phi}_k \mathbf{P}_{k-1}^+ \boldsymbol{\Phi}_k^\mathrm{T} + \mathbf{Q}_k \tag{4.5}$$

The measurement error $\boldsymbol{v}_k$ is defined as the difference between the actual measurement $\boldsymbol{z}_k$, and the estimated measurement $\hat{\boldsymbol{z}}_k$

$$\boldsymbol{v}_k = \boldsymbol{z}_k - \hat{\boldsymbol{z}}_k \tag{4.6}$$

$$\boldsymbol{v}_k = \boldsymbol{z}_k - \mathbf{C}_k \delta\hat{\boldsymbol{x}}_k^- \tag{4.7}$$

The covariance of the measurement error is

$$\mathbf{R}_k = \mathrm{E}[(\boldsymbol{z}_\mathrm{k} - \hat{\boldsymbol{z}}_\mathrm{k})(\boldsymbol{z}_\mathrm{k} - \hat{\boldsymbol{z}}_\mathrm{k})^\mathrm{T}] \tag{4.8}$$

Since the filter state estimates $\delta\hat{\boldsymbol{x}}$ are reset to zero after updating the reference state, the measurement error $\boldsymbol{v}_k$ is the same as the measurement $\boldsymbol{z}_k$ in this application.

After obtaining the $k$th measurement, the estimated state is updated using

$$\delta\hat{\boldsymbol{x}}_k^+ = \delta\hat{\boldsymbol{x}}_k^- + \mathbf{K}_k\boldsymbol{v}_k \tag{4.9}$$

where the Kalman gain matrix $\mathbf{K}_k$ in (4.9) is defined as

$$\mathbf{K}_k = \mathbf{P}_k^-\mathbf{C}_k(\mathbf{C}_k^{\mathrm{T}}\mathbf{P}_k^-\mathbf{C}_k + \mathbf{R}_k)^{-1} \tag{4.10}$$

The covariance matrix is also updated using the Kalman gain matrix,

$$\mathbf{P}_k^+ = (\mathbf{I} - \mathbf{K}_k\mathbf{C}_k)\mathbf{P}_k^- \tag{4.11}$$

## 4.2 State Transition Equations

The equations of state for a general rotating body can be written as

$$\frac{d\boldsymbol{r}_I}{dt} = \boldsymbol{v}_I \tag{4.12}$$

$$\frac{d\boldsymbol{v}_I}{dt} = \mathbf{A}_{IB}\boldsymbol{s}_B + \boldsymbol{g}_I \tag{4.13}$$

$$\frac{d\mathbf{A}_{IB}}{dt} = \mathbf{A}_{IB}[\boldsymbol{\omega}_B\times] \tag{4.14}$$

$$\frac{d\boldsymbol{\omega}_B}{dt} = \boldsymbol{\alpha}_B \tag{4.15}$$

where $\boldsymbol{r}_I$ is the inertial position of the body, $\boldsymbol{v}_I$ is the velocity, $\boldsymbol{s}_B$ is the acceleration from specific force in the body-fixed reference frame, $\boldsymbol{\omega}_B$ is the angular rate of the body frame, $\boldsymbol{\alpha}_B$ is the angular acceleration, and the matrix $\mathbf{A}_{IB}$ is a $3 \times 3$ rotation matrix from the body to the inertial frame. The reverse rotation can be obtained using

$$\mathbf{A}_{IB}^{-1} = \mathbf{A}_{IB}^{\mathrm{T}} = \mathbf{A}_{BI} \tag{4.16}$$

since $\mathbf{A}_{IB}$ is orthonormal.

Note that in (4.15), $\boldsymbol{\omega}_B$ has been included as a state. This is unusual in an inertial navigation problem, where typically the body rate is taken directly from gyro measurements. In the accelerometer-only case, no direct rate measurement is available, so the rate must be estimated along with the other states.

The states $\boldsymbol{x}$ in (4.12–4.15) are treated as having small perturbations about a reference state $\bar{\boldsymbol{x}}$, so that $\boldsymbol{r}_I = \bar{\boldsymbol{r}}_I + \delta\boldsymbol{r}_I$, with equivalent expressions for the velocity, $\boldsymbol{v}_I$, and angular rate, $\boldsymbol{\omega}_B$. The attitude is written as the product of the reference attitude $\bar{\mathbf{A}}_{IB}$ and a small rotation $\boldsymbol{\psi}_B$ in the body frame, giving

$$\mathbf{A}_{IB} = \bar{\mathbf{A}}_{IB}(\mathbf{I} + [\boldsymbol{\psi}_B\times]) \tag{4.17}$$

This can be rewritten in terms of the reference attitude by recognizing that

$$\bar{\mathbf{A}}_{IB} = \mathbf{A}_{IB}(\mathbf{I} + [\boldsymbol{\psi}_B\times])^{-1} \tag{4.18}$$

$$\simeq \mathbf{A}_{IB}(\mathbf{I} + [\boldsymbol{\psi}_B\times])^{\mathrm{T}} \tag{4.19}$$

$$\simeq \mathbf{A}_{IB}(\mathbf{I} - [\boldsymbol{\psi}_B\times]) \tag{4.20}$$

### 4.2.1 Position Perturbation State

The differential equation for position can be written as

$$\frac{d(\bar{\boldsymbol{r}}_I + \delta \boldsymbol{r}_I)}{dt} = \boldsymbol{v}_I \tag{4.21}$$

Substituting for $\boldsymbol{v}_I$ and differentiating,

$$\bar{\boldsymbol{v}}_I + \frac{d(\delta \boldsymbol{r}_I)}{dt} = \bar{\boldsymbol{v}}_I + \delta \boldsymbol{v}_I \tag{4.22}$$

leaves the desired equation for the position perturbation,

$$\frac{d(\delta \boldsymbol{r}_I)}{dt} = \delta \boldsymbol{v}_I \tag{4.23}$$

### 4.2.2 Velocity Perturbation State

The equation for velocity is written as

$$\frac{d(\bar{\boldsymbol{v}}_I + \delta \boldsymbol{v}_I)}{dt} = \mathbf{A}_{IB}\boldsymbol{s}_B + \boldsymbol{g}_I \tag{4.24}$$

Differentiating and expanding the right hand side results in[1]

$$\bar{\mathbf{A}}_{IB}\bar{\boldsymbol{s}}_B + \bar{\boldsymbol{g}}_I + \frac{d(\delta \boldsymbol{v}_I)}{dt} = \bar{\mathbf{A}}_{IB}(\mathbf{I} + [\boldsymbol{\psi}_B\times])(\bar{\boldsymbol{s}}_B + \delta \boldsymbol{s}_B) + \boldsymbol{g}_I \tag{4.25}$$

$$\frac{d(\delta \boldsymbol{v}_I)}{dt} = \bar{\mathbf{A}}_{IB}[\boldsymbol{\psi}_B\times](\bar{\boldsymbol{s}}_B + \delta \boldsymbol{s}_B) + \bar{\mathbf{A}}_{IB}\delta \boldsymbol{s}_B \tag{4.26}$$

where $\delta \boldsymbol{s}_B$ comes from the specific force perturbation. Taking only first order terms and rearranging slightly leaves the equation for the velocity perturbation,

$$\frac{d(\delta \boldsymbol{v}_I)}{dt} = -\bar{\mathbf{A}}_{IB}[\bar{\boldsymbol{s}}_B\times]\boldsymbol{\psi}_B + \bar{\mathbf{A}}_{IB}\delta \boldsymbol{s}_B \tag{4.27}$$

### 4.2.3 Attitude Perturbation State

From (4.14), the differential equation for the attitude is

$$\frac{d\mathbf{A}_{IB}}{dt} = \mathbf{A}_{IB}[\boldsymbol{\omega}_B\times] \tag{4.28}$$

which can be compared to the result obtained from direct differentiation,

$$\frac{d\mathbf{A}_{IB}}{dt} = \frac{d(\bar{\mathbf{A}}_{IB}\{\mathbf{I} + [\boldsymbol{\psi}_B\times]\})}{dt} \tag{4.29}$$

[1] It is assumed here that the gravity term $\boldsymbol{g}_I$ is constant, so that $\delta \boldsymbol{g}_I = 0$, or $\boldsymbol{g}_I = \bar{\boldsymbol{g}}_I$

The right hand side of the first equation can be expanded to include perturbation terms:

$$\frac{d\mathbf{A}_{IB}}{dt} = \bar{\mathbf{A}}_{IB}(\mathbf{I} + [\psi_B\times])([\bar{\omega}_B\times] + [\delta\boldsymbol{\omega}_B\times]) \tag{4.30}$$

Differentiating the second equation,

$$\frac{d\mathbf{A}_{IB}}{dt} = \bar{\mathbf{A}}_{IB}[\frac{d\psi_B}{dt}\times] + \bar{\mathbf{A}}_{IB}[\bar{\omega}_B\times](\mathbf{I} + [\psi_B\times]) \tag{4.31}$$

and combining the two gives

$$(\mathbf{I} + [\psi_B\times])([\bar{\omega}_B\times] + [\delta\boldsymbol{\omega}_B\times]) = [\frac{d\psi_B}{dt}\times] + [\bar{\omega}_B\times](\mathbf{I} + [\psi_B\times]) \tag{4.32}$$

Taking only first order terms leaves

$$[\psi_B\times][\bar{\omega}_B\times] + [\delta\boldsymbol{\omega}_B\times] = [\frac{d\psi_B}{dt}\times] + [\bar{\omega}_B\times][\psi_B\times] \tag{4.33}$$

This can be further reduced by noting the matrix identity

$$[\bar{\omega}_B\times][\psi_B\times] - [\psi_B\times][\bar{\omega}_B\times] = [(\bar{\omega}_B \times \psi_B)\times] \tag{4.34}$$

Applying the identity and converting to vector form gives the desired equation for the attitude perturbation[2]

$$\frac{d\psi_B}{dt} = -[\bar{\omega}_B\times]\psi_B + \delta\boldsymbol{\omega}_B \tag{4.35}$$

### 4.2.4 Rate Perturbation State

The differential equation for the angular rate is

$$\frac{d(\bar{\omega}_B + \delta\boldsymbol{\omega}_B)}{dt} = \boldsymbol{\alpha}_B \tag{4.36}$$

Differentiating and expanding the right hand side

$$\bar{\boldsymbol{\alpha}}_B + \frac{d(\delta\boldsymbol{\omega}_B)}{dt} = \bar{\boldsymbol{\alpha}}_B + \delta\boldsymbol{\alpha}_B \tag{4.37}$$

leaves the desired equation for the rate perturbation

$$\frac{d(\delta\boldsymbol{\omega}_B)}{dt} = \delta\boldsymbol{\alpha}_B \tag{4.38}$$

---

[2]Attitude perturbations in inertial navigation are more often expressed in the *inertial* frame

$$\mathbf{A}_{IB} = (\mathbf{I} + [\psi_I\times])\bar{\mathbf{A}}_{IB}$$

which, after similar manipulation, results in a dynamical equation of the form

$$\frac{d\psi_I}{dt} = [\bar{\omega}_I\times]\psi_I + \delta\omega_I$$

The choice of the body-frame representation chosen here will become apparent in Section 5.3, where the derived gravity-turn alignment measurement can be considered a *direct* measurement of $\psi_B$

### 4.2.5 Instrument Errors

Perturbations of the specific force and angular acceleration vectors required in (4.27) and (4.38) can be written as functions of the accelerometer outputs,

$$\begin{aligned} \delta \boldsymbol{s}_B &= \mathbf{E}_1 \delta \boldsymbol{f} \\ \delta \boldsymbol{\alpha}_B &= \mathbf{E}_2 \delta \boldsymbol{f} \end{aligned} \tag{4.39}$$

where $\mathbf{E}_1$ and $\mathbf{E}_2$ are the matrix partitions introduced in (3.10), and $\delta \boldsymbol{f}$ is the perturbation in accelerometer output

$$\delta \boldsymbol{f} = \delta \boldsymbol{\beta} + \boldsymbol{\nu}_f \tag{4.40}$$

The perturbation in (4.40) is the uncompensated accelerometer measurement bias $\delta \boldsymbol{\beta}$ plus a noise process $\boldsymbol{\nu}_f$. This noise process can be modelled as the sum of quantization errors and a white noise process. Quantization errors are assumed to be uniformly distributed over the quantization interval $q$. For an accelerometer with $n$ bit output over a range of $\pm a$, the measurement error due to quantization over the range $\pm q/2$ can be characterized by

$$\sigma_q = \frac{a}{2^n \sqrt{3}} \tag{4.41}$$

where the quantization interval $q$ is given by

$$q = \frac{2a}{2^n} \tag{4.42}$$

Assuming an additional random walk term $\sigma_{rw}$, the covariance matrix for the accelerometer outputs $\mathbf{Q}_f = \mathrm{E}[\boldsymbol{\nu}_\mathrm{f} \boldsymbol{\nu}_\mathrm{f}^\mathrm{T}]$ can be written as

$$\mathbf{Q}_f = (\sigma_q^2 + \sigma_{rw}^2)\mathbf{I} \tag{4.43}$$

Combining the filter state equations, the state transition equation can be written in matrix form as

$$\frac{d}{dt}\begin{bmatrix} \delta \boldsymbol{r}_I \\ \delta \boldsymbol{v}_I \\ \boldsymbol{\psi}_B \\ \delta \boldsymbol{\omega}_B \\ \delta \boldsymbol{\beta} \end{bmatrix} = \begin{bmatrix} 0 & \mathbf{I} & 0 & 0 & 0 \\ 0 & 0 & -\bar{\mathbf{A}}_{IB}[\bar{\boldsymbol{s}}_B \times] & 0 & \bar{\mathbf{A}}_{IB}\mathbf{E}_1 \\ 0 & 0 & -[\bar{\boldsymbol{\omega}}_B \times] & \mathbf{I} & 0 \\ 0 & 0 & 0 & 0 & \mathbf{E}_2 \\ 0 & 0 & 0 & 0 & 0 \end{bmatrix} \begin{bmatrix} \delta \boldsymbol{r}_I \\ \delta \boldsymbol{v}_I \\ \boldsymbol{\psi}_B \\ \delta \boldsymbol{\omega}_B \\ \delta \boldsymbol{\beta} \end{bmatrix} + \begin{bmatrix} 0 \\ \bar{\mathbf{A}}_{IB}\mathbf{E}_1 \\ 0 \\ \mathbf{E}_2 \\ 0 \end{bmatrix} \boldsymbol{\nu}_f + \begin{bmatrix} \boldsymbol{\nu}_r \\ \boldsymbol{\nu}_v \\ \boldsymbol{\nu}_\psi \\ \boldsymbol{\nu}_\omega \\ \boldsymbol{\nu}_\beta \end{bmatrix} \tag{4.44}$$

or more compactly as

$$\frac{d(\delta \boldsymbol{x})}{dt} = \mathbf{F}\delta \boldsymbol{x} + \mathbf{E}_A \boldsymbol{\nu}_f + \boldsymbol{\nu}_s \tag{4.45}$$

where $\boldsymbol{\nu}_s$ has been included as an optional additional white noise process for each of the filter states. Since the process noise in (4.45) has zero mean, the state transition equation (4.3) can be approximated by

$$\Phi_k = e^{\mathbf{F}\Delta t} \approx (\mathbf{I} + \mathbf{F}\Delta t) \tag{4.46}$$

$$\delta \hat{\boldsymbol{x}}_k = \Phi_k \delta \hat{\boldsymbol{x}}_{k-1} \tag{4.47}$$

The covariance propagation equation of (4.5) becomes

$$\mathbf{P}_k^- = \Phi_k \mathbf{P}_{k-1}^+ \Phi_k^{\mathrm{T}} + \mathbf{Q}_E + \mathbf{Q}_s \tag{4.48}$$

where the covariance noise matrix $\mathbf{Q}_k$ has be separated into two components. The first is an effect of the accelerometer sensors noise:

$$\mathbf{Q}_f = \mathbf{E}_A \mathbf{Q}_f \mathbf{E}_A^{\mathrm{T}} \tag{4.49}$$

and the second comes from the additional process noise term $\boldsymbol{\nu}_s$:

$$\mathbf{Q}_s = \mathrm{E}[\boldsymbol{\nu}_s \boldsymbol{\nu}_s^{\mathrm{T}}] \tag{4.50}$$

### 4.2.6 Effect of Sensor Misalignments

An important error source not explicitly modelled in the filter is the effect of sensor misalignments. A misalignment in an accelerometer which is nominally aligned with the vehicle spin axis will experience a very large unmodelled disturbance due to centripetal acceleration effects. The following calculation shows how this error may be partially mitigated through bias estimation. Taking the instrument output transformation (3.6), the output of a given accelerometer is

$$f_i = \boldsymbol{\theta}_i^{\mathrm{T}} \boldsymbol{s}_B - \boldsymbol{\theta}_i^{\mathrm{T}} [\boldsymbol{r}_i \times] \boldsymbol{\alpha}_B + \boldsymbol{m}^{\mathrm{T}} \boldsymbol{w}_c + \boldsymbol{n}^{\mathrm{T}} \boldsymbol{w}_s \tag{4.51}$$

Defining the matrix permutations of the position vector $\boldsymbol{r}_i$

$$\mathbf{R}_m = \begin{bmatrix} r_{i_2} & r_{i_1} & 0 \\ r_{i_3} & 0 & r_{i_1} \\ 0 & r_{i_3} & r_{i_2} \end{bmatrix} \qquad \mathbf{R}_n = \begin{bmatrix} r_{i_1} & 0 & 0 \\ 0 & r_{i_2} & 0 \\ 0 & 0 & r_{i_3} \end{bmatrix} \tag{4.52}$$

the accelerometer output may be rewritten as

$$\begin{aligned} f_i &= \boldsymbol{\theta}_i^{\mathrm{T}} \boldsymbol{s}_B - \boldsymbol{\theta}_i^{\mathrm{T}} [\boldsymbol{r}_i \times] \boldsymbol{\alpha}_B + (\mathbf{R}_m \boldsymbol{\theta}_i)^{\mathrm{T}} \boldsymbol{w}_c + (\mathbf{R}_n \boldsymbol{\theta}_i)^{\mathrm{T}} \boldsymbol{w}_s & (4.53) \\ &= \boldsymbol{\theta}_i^{\mathrm{T}} (\boldsymbol{s}_B - [\boldsymbol{r}_i \times] \boldsymbol{\alpha}_B + \mathbf{R}_m^{\mathrm{T}} \boldsymbol{w}_c + \mathbf{R}_n \boldsymbol{w}_s) & (4.54) \end{aligned}$$

Define now a small misalignment $\boldsymbol{\lambda}_i$ of the orientation vector $\boldsymbol{\theta}_i$, so that

$$\boldsymbol{\theta}_i = (\mathbf{I} + [\boldsymbol{\lambda}_i \times]) \bar{\boldsymbol{\theta}}_i \tag{4.55}$$

The output error resulting from this misalignment is

$$\kappa_i = -\bar{\boldsymbol{\theta}}_i^{\mathrm{T}} [\boldsymbol{\lambda}_i \times] \begin{bmatrix} \mathbf{I} & -[\boldsymbol{r}_i \times] & \mathbf{R}_m^{\mathrm{T}} & \mathbf{R}_n \end{bmatrix} \begin{bmatrix} \boldsymbol{s}_B \\ \boldsymbol{\alpha}_B \\ \boldsymbol{w}_c \\ \boldsymbol{w}_s \end{bmatrix} \tag{4.56}$$

This can be greatly simplified if it can be assumed that terms resulting from lateral forces, accelerations, and rates will approximately cancel over a single revolution, the

angular acceleration about the spin axis is small, and that $\boldsymbol{w}_s$ is dominated by the $\omega_x^2$ term. In an average sense, the error resulting from sensor misalignment is roughly

$$\langle \kappa_i \rangle \approx -\bar{\boldsymbol{\theta}}_i^{\mathrm{T}} [\boldsymbol{\lambda}_i \times] \left( \begin{bmatrix} a_{c_x} \\ 0 \\ 0 \end{bmatrix} + \mathbf{R}_n \begin{bmatrix} 0 \\ -\omega_x^2 \\ -\omega_x^2 \end{bmatrix} \right) \tag{4.57}$$

This expression looks much like a bias, particularly in situations with high spin rates and low drag. The effect of misalignment on rate estimation, and the effectiveness of bias state compensation, is discussed in Section 6.1.3.

## 4.3 Measurement Equations

The state transition equations defined in (4.44) for the perturbation states use accelerometer outputs for calculation of the specific force vector $\boldsymbol{s}_B$ and the angular acceleration $\boldsymbol{\alpha}_B$. Additional information can be obtained about the angular rates by considering the measured values of the rate products defined in (3.10). This gives two vector measurements which can be used as a check on the integration of $\boldsymbol{\alpha}_B$. Additionally, data from an external source such as GPS may be available for state estimation. These measurements have a direct use in estimating the vehicle position and velocity, and also provide an indirect means of estimating vehicle orientation. In the absence of GPS, trajectory information from a pre-computed fire-control solution can be substituted to aide in the dynamics-based navigation measurements presented in Chapter 5.

### 4.3.1 Rate Measurements

The rate products in (3.10) can be used as measurements by taking the difference between these values and the products of the reference rates in the navigation filter. In the following, these measurements are represented as two different vectors, one with the rate cross terms, the other with the square terms. Beginning with the cross rate terms, the measurement can be constructed as

$$\boldsymbol{z}_{\omega C} = \mathbf{E}_3 \bar{\boldsymbol{f}} - \begin{bmatrix} \bar{\omega}_x \bar{\omega}_y \\ \bar{\omega}_x \bar{\omega}_z \\ \bar{\omega}_y \bar{\omega}_z \end{bmatrix} \tag{4.58}$$

This can be rewritten in terms of the rate perturbation $\delta\boldsymbol{\omega}_B$ and the uncompensated bias $\delta\boldsymbol{\beta}$. Thus

$$\boldsymbol{z}_{\omega C} = \mathbf{E}_3(\boldsymbol{f} - \delta\boldsymbol{\beta}) - \begin{bmatrix} (\omega_x - \delta\omega_x)(\omega_y - \delta\omega_y) \\ (\omega_x - \delta\omega_x)(\omega_z - \delta\omega_z) \\ (\omega_y - \delta\omega_y)(\omega_z - \delta\omega_z) \end{bmatrix} \tag{4.59}$$

Taking partials with respect to the filter states and keeping only first order terms gives, for the rate

$$\mathbf{C}_{\omega C} \equiv \frac{\partial \boldsymbol{z}_{\omega C}}{\partial(\delta\boldsymbol{\omega}_B)} = \begin{bmatrix} \omega_y & \omega_x & 0 \\ \omega_z & 0 & \omega_x \\ 0 & \omega_z & \omega_y \end{bmatrix} \tag{4.60}$$

and for the instrument bias

$$\mathbf{C}_{\beta_C} \equiv \frac{\partial \boldsymbol{z}_{\omega_C}}{\partial(\delta\boldsymbol{\beta})} = -\mathbf{E}_3 \tag{4.61}$$

Similarly, for the squared rate terms the measurement may be constructed as

$$\boldsymbol{z}_{\omega_S} = \mathbf{E}_4\bar{\boldsymbol{f}} - \begin{bmatrix} -\bar{\omega}_y^2 - \bar{\omega}_z^2 \\ -\bar{\omega}_x^2 - \bar{\omega}_z^2 \\ -\bar{\omega}_x^2 - \bar{\omega}_y^2 \end{bmatrix} \tag{4.62}$$

which may once again be rewritten in terms of the true rates and rate perturbations

$$\boldsymbol{z}_{\omega_S} = \mathbf{E}_4(\boldsymbol{f} - \delta\boldsymbol{\beta}) + \begin{bmatrix} (\omega_y - \delta\omega_y)^2 + (\omega_z - \delta\omega_z)^2 \\ (\omega_x - \delta\omega_x)^2 + (\omega_z - \delta\omega_z)^2 \\ (\omega_x - \delta\omega_x)^2 + (\omega_y - \delta\omega_y)^2 \end{bmatrix} \tag{4.63}$$

The partial derivative matrices for this measurement are, to first order

$$\mathbf{C}_{\omega_S} \equiv \frac{\partial \boldsymbol{z}_{\omega_S}}{\partial(\delta\boldsymbol{\omega}_B)} = -2\begin{bmatrix} 0 & \omega_y & \omega_z \\ \omega_x & 0 & \omega_z \\ \omega_x & \omega_y & 0 \end{bmatrix} \tag{4.64}$$

for the rate, and

$$\mathbf{C}_{\beta_S} \equiv \frac{\partial \boldsymbol{z}_{\omega_S}}{\partial(\delta\boldsymbol{\beta})} = -\mathbf{E}_4 \tag{4.65}$$

for the instrument bias. Note, however, that the matrices defined in (4.60) and (4.64) require the *true* rates $\boldsymbol{\omega}_B$. Since these are obviously not known to the filter, it must make due with its best estimate of the rates, $\bar{\boldsymbol{\omega}}_B$.

The measurements can now be modelled as linear functions of the filter states

$$\begin{bmatrix} \boldsymbol{z}_{\omega_C} \\ \boldsymbol{z}_{\omega_S} \end{bmatrix} = \begin{bmatrix} 0 & 0 & 0 & \mathbf{C}_{\omega_C} & \mathbf{C}_{\beta_C} \\ 0 & 0 & 0 & \mathbf{C}_{\omega_S} & \mathbf{C}_{\beta_S} \end{bmatrix} \begin{bmatrix} \delta\boldsymbol{r}_I \\ \delta\boldsymbol{v}_I \\ \boldsymbol{\psi}_B \\ \delta\boldsymbol{\omega}_B \\ \delta\boldsymbol{\beta} \end{bmatrix} + \begin{bmatrix} \boldsymbol{\nu}_{\omega_C} \\ \boldsymbol{\nu}_{\omega_S} \end{bmatrix} \tag{4.66}$$

where the measurement noise terms $\boldsymbol{\nu}_{\omega_C}$ and $\boldsymbol{\nu}_{\omega_S}$ come directly from the accelerometer noise error $\boldsymbol{\nu}_f$ in (4.45). Thus

$$\boldsymbol{\nu}_{\omega_C} = \mathbf{E}_3\boldsymbol{\nu}_f \tag{4.67}$$

$$\boldsymbol{\nu}_{\omega_S} = \mathbf{E}_4\boldsymbol{\nu}_f \tag{4.68}$$

The two vector measurements are correlated, and the combined measurement noise matrix $\mathbf{R}$ required in (4.10) can be expressed as

$$\mathbf{R}_\omega = \begin{bmatrix} \mathbf{E}_3 \\ \mathbf{E}_4 \end{bmatrix} \mathbf{Q}_f \begin{bmatrix} \mathbf{E}_3^{\mathrm{T}} & \mathbf{E}_4^{\mathrm{T}} \end{bmatrix} \tag{4.69}$$

### 4.3.2 GPS Measurement

If position and velocity measurements are available from GPS, or from an alternate source such as a pre-launch firing solution, then the measurement vector can be augmented to include these terms. First, the position and velocity measurements are constructed in terms of the reference values:

$$\boldsymbol{z}_r = \boldsymbol{r}_{gps} - \bar{\boldsymbol{r}}_I \tag{4.70}$$

$$\boldsymbol{z}_v = \boldsymbol{v}_{gps} - \bar{\boldsymbol{r}}_I \tag{4.71}$$

where $\boldsymbol{r}_{gps}$ and $\boldsymbol{v}_{gps}$ are from GPS or similar measurements. Rewriting in terms of the perturbation states,

$$\boldsymbol{z}_r = \boldsymbol{r}_{gps} - (\boldsymbol{r}_I - \delta\boldsymbol{r}_I) \tag{4.72}$$

$$\boldsymbol{z}_v = \boldsymbol{v}_{gps} - (\boldsymbol{v}_I - \delta\boldsymbol{v}_I) \tag{4.73}$$

The partial derivatives with respect to the filter states are

$$\frac{\partial \boldsymbol{z}_r}{\partial(\delta\boldsymbol{r}_I)} = \mathbf{I} \tag{4.74}$$

$$\frac{\partial \boldsymbol{z}_v}{\partial(\delta\boldsymbol{v}_I)} = \mathbf{I} \tag{4.75}$$

The measurement model is

$$\begin{bmatrix} \boldsymbol{z}_r \\ \boldsymbol{z}_v \end{bmatrix} = \begin{bmatrix} \mathbf{I} & 0 & 0 & 0 & 0 \\ 0 & \mathbf{I} & 0 & 0 & 0 \end{bmatrix} \begin{bmatrix} \delta\boldsymbol{r}_I \\ \delta\boldsymbol{v}_I \\ \boldsymbol{\psi}_B \\ \delta\boldsymbol{\omega}_B \\ \delta\boldsymbol{\beta} \end{bmatrix} + \begin{bmatrix} \boldsymbol{\nu}_r \\ \boldsymbol{\nu}_v \end{bmatrix} \tag{4.76}$$

and the measurement covariances for these two measurements are defined as

$$\mathbf{R}_r \equiv \mathrm{E}[\boldsymbol{\nu}_r \boldsymbol{\nu}_r^{\mathrm{T}}] = \sigma_r^2 \mathbf{I} \tag{4.77}$$

$$\mathbf{R}_v \equiv \mathrm{E}[\boldsymbol{\nu}_v \boldsymbol{\nu}_v^{\mathrm{T}}] = \sigma_v^2 \mathbf{I} \tag{4.78}$$

Combining the measurement equations for all measurement types gives the total matrix of measurement partials $\mathbf{C}$

$$\mathbf{C} = \begin{bmatrix} 0 & 0 & 0 & \mathbf{C}_{\omega C} & \mathbf{C}_{\beta C} \\ 0 & 0 & 0 & \mathbf{C}_{\omega S} & \mathbf{C}_{\beta S} \\ \mathbf{I} & 0 & 0 & 0 & 0 \\ 0 & \mathbf{I} & 0 & 0 & 0 \end{bmatrix} \tag{4.79}$$

and matrix of measurement error covariance $\mathbf{R}$

$$\mathbf{R} = \left[\begin{array}{c|cc} \mathbf{R}_\omega & 0 & \\ \hline 0 & \mathbf{R}_r & 0 \\ & 0 & \mathbf{R}_v \end{array}\right] \tag{4.80}$$

required in (4.10) and (4.11).

## 4.4 State Update Equations

### 4.4.1 Propagating the Reference State

The state transition matrix defined in (4.46) is defined for the filter states. Before applying the correction to the reference state found in the perturbation state calculation in (4.9), it is necessary to propagate the reference state to the next time step. This calculation is performed independently from and prior to the Kalman filter updates. The position, velocity, attitude quaternion, and angular rate can be defined as a 13 element state vector of the form

$$\boldsymbol{x} = \begin{bmatrix} \boldsymbol{r}_I \\ \boldsymbol{v}_I \\ \boldsymbol{q} \\ \boldsymbol{\omega}_B \end{bmatrix} \tag{4.81}$$

The reference states can be propagated using the specific force and angular acceleration terms defined in (3.9). The update equations for these states are

$$\bar{\boldsymbol{r}}_I \Leftarrow \bar{\boldsymbol{r}}_I + \bar{\boldsymbol{v}}_I \Delta t \tag{4.82}$$

$$\bar{\boldsymbol{v}}_I \Leftarrow \bar{\boldsymbol{v}}_I + (\boldsymbol{g}_I + \bar{\mathbf{A}}_{IB}\boldsymbol{s}_B)\Delta t \tag{4.83}$$

$$\bar{\boldsymbol{\omega}}_B \Leftarrow \bar{\boldsymbol{\omega}}_B + \boldsymbol{\alpha}_B \Delta t \tag{4.84}$$

A very simple form for the attitude update takes the rate as a constant over the integration interval. The attitude quaternion is written as a rotation from the inertial frame to the body frame. The quaternion is defined with vector part $\boldsymbol{q}_v$ and scalar part $q_s$ such that $\boldsymbol{q} = [\boldsymbol{q}_v, q_s]$, following the convention in [10] . For a short time step, the quaternion update can be approximated by

$$\bar{\boldsymbol{q}} \Leftarrow \left( \mathbf{I} + \frac{1}{2} \begin{bmatrix} 0 & \bar{\omega}_z & -\bar{\omega}_y & \bar{\omega}_x \\ -\bar{\omega}_z & 0 & \bar{\omega}_x & \bar{\omega}_y \\ \bar{\omega}_y & -\bar{\omega}_x & 0 & \bar{\omega}_z \\ -\bar{\omega}_x & -\bar{\omega}_y & -\bar{\omega}_z & 0 \end{bmatrix} \Delta t \right) \bar{\boldsymbol{q}} \tag{4.85}$$

The quaternion at the midpoint of the timestep $\Delta t$ should be used to calculate the reference attitude $\bar{\mathbf{A}}_{IB}^{\mathrm{T}}$ required in (4.45) and (4.83). This can be found be replacing $\Delta t$ with $\frac{\Delta t}{2}$ in (4.85). The $3\times3$ rotation matrix $\mathbf{A}_{IB}^{\mathrm{T}}$ can then be found by transforming the quaternion to matrix form

$$\mathbf{A}_{IB}^{\mathrm{T}} = (q_s^2 - \boldsymbol{q}_v^{\mathrm{T}}\boldsymbol{q}_v)\mathbf{I} + 2\boldsymbol{q}_v\boldsymbol{q}_v^{\mathrm{T}} - 2q_s[\boldsymbol{q}_v\times] \tag{4.86}$$

### 4.4.2 Applying the Error States

Once the reference state has been propagated to the new time step, the filter states can be applied. Since state perturbations were defined as positive quantities in Section

4.2, the state corrections for position, velocity, angular rate, and bias are just

$$\bar{\boldsymbol{r}}_I \Leftarrow \bar{\boldsymbol{r}}_I + \delta\hat{\boldsymbol{r}}_I \tag{4.87}$$

$$\bar{\boldsymbol{v}}_I \Leftarrow \bar{\boldsymbol{v}}_I + \delta\hat{\boldsymbol{v}}_I \tag{4.88}$$

$$\bar{\boldsymbol{\omega}}_B \Leftarrow \bar{\boldsymbol{\omega}}_B + \delta\hat{\boldsymbol{\omega}}_B \tag{4.89}$$

$$\bar{\boldsymbol{\beta}} \Leftarrow \bar{\boldsymbol{\beta}} + \delta\hat{\boldsymbol{\beta}} \tag{4.90}$$

The attitude correction in matrix form comes from (4.17)

$$\bar{\mathbf{A}}_{IB} \Leftarrow \bar{\mathbf{A}}_{IB}(\mathbf{I} + [\hat{\boldsymbol{\psi}}_B\times]) \tag{4.91}$$

However, since the reference attitude attitude state is a quaternion, the correction must be made in this form. Defining the correction rotation as

$$\hat{\boldsymbol{q}}_\psi \approx [\hat{\boldsymbol{\psi}}_B, 1] \tag{4.92}$$

the attitude correction becomes

$$\bar{\boldsymbol{q}} \Leftarrow \bar{\boldsymbol{q}} \cdot \hat{\boldsymbol{q}}_\psi \tag{4.93}$$

where the quaternion multiplication operation is defined as

$$\boldsymbol{q}_1 \cdot \boldsymbol{q}_2 = [(\boldsymbol{q}_{1v} \times \boldsymbol{q}_{2v} + q_{2s}\boldsymbol{q}_{1v} + q_{1s}\boldsymbol{q}_{2v}), (q_{1s}q_{2s} - \boldsymbol{q}_{1v} \cdot \boldsymbol{q}_{2v})] \tag{4.94}$$

## 4.5 Managing Rate Linearization Error

Since the filter scheme proposed is an extended Kalman filter, stability of the rate estimate is not guaranteed, since calculation of measurement partials in (4.60) and (4.64) depends on the filter's own rate estimate. If the rate estimation error is large, the error in $\mathbf{C}$ will also be large, leading very quickly to filter divergence. This problem is particulary acute during filter initialization, since the initial rate may not be well known. The problem is most notable in cases with large initial biases, or large sensor noises.

As noted in [3], most proposed solutions to this problem are based on ad-hoc numerical tricks and are not easily generalized. In the current problem, several modifications to the filter can be made to help reduce the risk of divergence in the first few filter updates. These modifications will be referred to collectively as *EKF compensation.*

The first modification is to construct the $\mathbf{C}$ matrices of (4.60) and (4.64) based on a *nominal* rate $\boldsymbol{\omega}_{nom}$, rather than the reference rate $\bar{\boldsymbol{\omega}}$. This approximation helps to prevent a large transient estimation error from causing divergence. In the final form of the navigation filter, this approximation was made for the first 1/10 sec (10 filter steps), and was done only to the roll rate, since this is by far the largest rate component.

The second modification scales the measurement noise matrix by a constant factor $k$. also for the initial 1/10 sec. This modification causes the filter to make smaller initial rate corrections over the first few steps. This is necessary since the initial covariance matrix $\mathbf{P}_0^-$ is relatively large, and the angular rate error might otherwise

make a very large jump in the first step. A value of $k = 100$ was found to give reasonably good results in most cases.

A further modification was needed in cases with very low sensor noise. Even with the above-mentioned compensation techniques, filter performance would deteriorate for $\sigma_{rw}$ values less than about 0.5 milli-g/$\sqrt{\text{Hz}}$. For this reason, unless otherwise noted, the value of $\sigma_{rw}$ used in the filter was lower bounded to 1.5 milli-g/$\sqrt{\text{Hz}}$, even in cases where significantly better instrument performance was modelled.

# Chapter 5

# Dynamics Based Navigation

Without an external reference such as GPS, the attitude determination problem cannot be solved using standard navigation techniques, since no initial roll attitude estimate is available to the navigation algorithm. This is true even in the error-free case, since accelerometers alone can only provide information about *changes* in vehicle orientation through rate estimation. However, an attitude estimate may still be made by exploiting the known dynamics of the vehicle. Specifically, the vehicle is expected to pitch over during flight to maintain alignment of its nose with the wind-relative velocity vector. This vector alignment can serve to correct attitude errors in vehicle pitch and yaw relative to its heading. Additionally, if the pitch-over rate could be separated from the larger lateral rates from vehicle dynamics, a second measurement could be obtained by aligning the expected pitch-over rate vector with the transverse component of vehicle rate[1]. This vector alignment would serve to correct attitude errors about the vehicle spin axis. Vehicle roll orientation is by far the most difficult state to estimate, which is why this type of navigation problem is sometimes referred to as *down-determination.*

## 5.1 Gravity Turn Rate

Taking velocity components in the vertical plane defined by the flight path, a simple model for the velocity is

$$\boldsymbol{v} = v \begin{bmatrix} \cos\gamma \\ \sin\gamma \end{bmatrix} \tag{5.1}$$

where $\gamma$ is the flight path angle measured from the horizontal plane. Differentiation with respect to time gives

$$\dot{\boldsymbol{v}} = \dot{v} \begin{bmatrix} \cos\gamma \\ \sin\gamma \end{bmatrix} + \dot{\gamma} v \begin{bmatrix} -\sin\gamma \\ \cos\gamma \end{bmatrix} \tag{5.2}$$

which separates the acceleration of the body into components in the lift and drag directions. The rate of change of velocity in the absence of lateral aerodynamic forces

[1]Since dynamics-based navigation is necessitated by the lack of external measurements, velocity alignment and pitch-over reference vectors must come from a pre-launch firing solution for the projectile.

can also be written as

$$\dot{\boldsymbol{v}} = \begin{bmatrix} 0 \\ -g \end{bmatrix} \tag{5.3}$$

The rate of change of the flight path angle $\dot{\gamma}$ is the pitch-over rate, which can be isolated by recognizing that the two vectors on the right hand side of (5.2) are orthogonal unit vectors. Taking dot products of both sides with the second of these two vectors gives

$$\dot{\gamma} = \frac{-g\cos\gamma}{v} \tag{5.4}$$

## 5.2 Velocity Alignment Pseudo-Measurement

Information about the vehicle attitude can be obtained from a velocity estimate if it is assumed that the nose of the vehicle is aligned with the velocity vector. This is a reasonable approximation as long as there are negligible winds and the vehicle angle of attack is *assumed to be very small.* This amounts to a measurement of the difference between the nose of the vehicle and the reference unit velocity vector. The unit velocity vector in the inertial frame is

$$\boldsymbol{i}_v = \frac{\bar{\boldsymbol{v}}_I}{|\bar{\boldsymbol{v}}_I|} \tag{5.5}$$

Assuming that the nose of the vehicle is aligned with the body x-axis, the unit vector along the nose of the vehicle can simply be expressed in body coordinates as

$$\boldsymbol{i}_x = \begin{bmatrix} 1 & 0 & 0 \end{bmatrix}^{\mathrm{T}} \tag{5.6}$$

### Inertial Frame

The pointing misalignment measurement can be constructed by rotating $\boldsymbol{i}_x$ into the inertial frame, and taking the difference with the inertial velocity vector

$$\boldsymbol{z}_{mis} = \boldsymbol{i}_v - \bar{\mathbf{A}}_{IB}\boldsymbol{i}_x \tag{5.7}$$

Expanding the attitude into its component states, the misalignment measurement becomes

$$\boldsymbol{z}_{mis} = \boldsymbol{i}_v - \mathbf{A}_{IB}(\mathbf{I} - [\boldsymbol{\psi}_B\times])\boldsymbol{i}_x \tag{5.8}$$

This can be rearranged to isolate the component due to the attitude perturbation

$$\boldsymbol{z}_{mis} = \boldsymbol{i}_v - \mathbf{A}_{IB}\boldsymbol{i}_x - \mathbf{A}_{IB}[\boldsymbol{i}_x\times]\boldsymbol{\psi}_B \tag{5.9}$$

Taking the partial derivative of this measurement with respect to the attitude perturbation term gives

$$\mathbf{C}_{mis,\psi} \equiv \frac{\partial \boldsymbol{z}_{mis}}{\partial \boldsymbol{\psi}_B} = -\mathbf{A}_{IB}[\boldsymbol{i}_x\times] \tag{5.10}$$

Note that since

$$[\boldsymbol{i}_x\times] = \begin{bmatrix} 0 & 0 & 0 \\ 0 & 0 & -1 \\ 0 & 1 & 0 \end{bmatrix} \tag{5.11}$$

this amounts to a shuffling of the columns of $\mathbf{A}_{IB}$. While quite simple, this representation of the misalignment vector has the drawback that the measurement error covariance matrix must be given in inertial coordinates. A more natural expression for the misalignment can be found by formulating the measurement in the body frame.

### Body Frame

The misalignment measurement defined in the body frame is

$$\boldsymbol{z}_{mis} = \bar{\mathbf{A}}_{IB}^{\mathrm{T}}\boldsymbol{i}_v - \boldsymbol{i}_x \tag{5.12}$$

Expanding,

$$\boldsymbol{z}_{mis} = (\mathbf{I} + [\boldsymbol{\psi}_B\times])\mathbf{A}_{IB}^{\mathrm{T}}\boldsymbol{i}_v - \boldsymbol{i}_x \tag{5.13}$$

$$\boldsymbol{z}_{mis} = \mathbf{A}_{IB}^{\mathrm{T}}\boldsymbol{i}_v + [\boldsymbol{\psi}_B\times]\mathbf{A}_{IB}^{\mathrm{T}}\boldsymbol{i}_v - \boldsymbol{i}_x \tag{5.14}$$

Taking the partial derivative with respect to the attitude perturbation gives

$$\mathbf{C}_{mis,\psi} \equiv \frac{\partial \boldsymbol{z}_{mis}}{\partial \boldsymbol{\psi}_B} = -[(\mathbf{A}_{IB}^{\mathrm{T}}\boldsymbol{i}_v)\times] \tag{5.15}$$

For both cases, the measurement model is then

$$\boldsymbol{z}_{mis} = \begin{bmatrix} 0 & 0 & \mathbf{C}_{mis,\psi} & 0 & 0 \end{bmatrix} \begin{bmatrix} \delta\boldsymbol{r}_I \\ \delta\boldsymbol{v}_I \\ \boldsymbol{\psi}_B \\ \delta\boldsymbol{\omega}_B \\ \delta\boldsymbol{\beta} \end{bmatrix} + \boldsymbol{\nu}_{mis} \tag{5.16}$$

The advantage of the body frame formulation is now apparent, as the covariance of the measurement error $\boldsymbol{\nu}_{mis}$ can now be expressed as

$$\mathbf{R}_{v_{mis}} = \mathrm{E}[\boldsymbol{\nu}_{mis}\boldsymbol{\nu}_{mis}^{\mathrm{T}}] = \begin{bmatrix} \sigma_x & 0 & 0 \\ 0 & \sigma_{mis} & 0 \\ 0 & 0 & \sigma_{mis} \end{bmatrix} \tag{5.17}$$

This matrix can be constructed prior to flight, and is constant, whereas the inertial form of the measurement would require a dynamic calculation of the form

$$\mathbf{R}_{v_{mis}} = \mathbf{A}_{IB}\mathrm{E}[\boldsymbol{\nu}_{mis}\boldsymbol{\nu}_{mis}^{\mathrm{T}}]\mathbf{A}_{IB}^{\mathrm{T}} \tag{5.18}$$

Note here that the upper left entry in (5.17) represents the uncertainty in the x-component of the vector measurement. Since the velocity alignment measurement really only gives information about the other two axes, only the lower 2×2 partition of the matrix should be used, along with the corresponding elements of the measurement defined in (5.12).

## 5.3 Gravity Turn Alignment Pseudo-Measurement

A second type of estimate of vehicle attitude might be made by noting that the vehicle should have a transverse rate component equal to (or at least parallel to) that found in (5.4). Assuming that the direction of the velocity vector is known, the direction of the flight-plane normal can be written as

$$\boldsymbol{i}_{\dot{\gamma}} = \frac{\boldsymbol{v}_I \times \boldsymbol{i}_z}{|\boldsymbol{v}_I \times \boldsymbol{i}_z|} \tag{5.19}$$

The transverse component of angular rate can be found by taking the last two components of vehicle angular rate in the body frame. Defining the matrix $\mathbf{I}_t$ as

$$\mathbf{I}_t = \begin{bmatrix} 0 & 0 & 0 \\ 0 & 1 & 0 \\ 0 & 0 & 1 \end{bmatrix} \tag{5.20}$$

the transverse component of angular rate in the body frame is $\mathbf{I}_t\boldsymbol{\omega}_B$. This can then be transformed to the inertial frame through multiplication by $\mathbf{A}_{IB}$.

The gravity turn pseudo-measurement could then be defined as the difference between the gravity turn vector expected from the known vehicle dynamics, and the expected lateral rate vector in inertial coordinates.

$$\boldsymbol{z}_{\dot{\gamma}} = \dot{\gamma}\boldsymbol{i}_{\dot{\gamma}} - \bar{\mathbf{A}}_{IB}\mathbf{I}_t\bar{\boldsymbol{\omega}}_B \tag{5.21}$$

This type of measurement formulation is extremely attractive, since it *seems* to provide a second vector measurement for attitude estimation which is orthogonal to the first. However, in practice this direct approach does not work, since lateral rates from precession are generally much greater than the gravity-turn rate, and will corrupt the measurement.

### 5.3.1 Isolating the Pitch-Over Rate Component

A modification of the above can be made to help isolate the low frequency pitch-over component of the lateral rates from the higher frequency dynamic components. It should first be noted that the pitch-over component of the lateral rate has constant direction in the aeroballistic frame, with magnitude roughly that found in (5.4). The lateral rate in this non-rotating frame can be found by first integrating the referemce roll rate:

$$\vartheta = \int_0^t \bar{\omega}_x(\tau)d\tau \tag{5.22}$$

and defining the transformation matrix

$$\boldsymbol{\Theta} \equiv \begin{bmatrix} 1 & 0 & 0 \\ 0 & \cos(\vartheta) & -\sin(\vartheta) \\ 0 & \sin(\vartheta) & \cos(\vartheta) \end{bmatrix} \tag{5.23}$$

so that the lateral rate in an intermediate frame fixed with respect to the aeroballistic frame is $\boldsymbol{\Theta}\mathbf{I}_t\boldsymbol{\omega}_B$. This quantity should have a secular component $\langle \mathbf{I}_t\boldsymbol{\omega}_B \rangle$ resulting from the pitch-over that indicates the direction of the local horizontal.

The secular component can be isolated by passing the estimated aeroballistic rate above through a low-pass digital filter $G$, and then transforming the filtered quantity back to the body frame. The result should be the pitch-over component of the estimated lateral rate in the body frame $\langle \mathbf{I}_t\bar{\boldsymbol{\omega}}_B \rangle$.

$$\mathbf{I}_t\bar{\boldsymbol{\omega}}_B \rightarrow \boxed{\boldsymbol{\Theta}} \rightarrow \boxed{G} \rightarrow \boxed{\boldsymbol{\Theta}^{\mathrm{T}}} \rightarrow \langle \mathbf{I}_t\bar{\boldsymbol{\omega}}_B \rangle \tag{5.24}$$

The rate filtering is done in the non-rolling frame defined by $\boldsymbol{\Theta}$ because the pitch-over component has constant direction in this frame, which allows the signal to be extracted using a low-pass filter. In the constant roll-rate case used in this thesis, it would also be possible to find the pitch-over component using a *band-pass* filter tuned to the expected roll rate of the projectile. However, this method would fail if the roll rate of the vehicle wandered out of the pass band of the filter. Filtering in the non-rolling frame avoids this problem, even with changes in the spin rate, as long as the estimated rates used in calculating $\boldsymbol{\Theta}$ are accurate.

The difficulty with this scheme comes when accelerometer biases are introduced into the system. Large biases may potentially cause a significant error in the estimated roll rates $\bar{\omega}_{B_x}$, resulting in errors in the transformation to the non-rolling frame through $\boldsymbol{\Theta}$. The filtered rate $\langle \mathbf{I}_t\bar{\boldsymbol{\omega}}_B \rangle$ will look like a slowly varying quantity, with frequency equal to the roll rate error, and with an error magnitude proportional to the phase lag of the filter at that frequency. Large corrections to the reference roll rate can upset the convergence of $\langle \mathbf{I}_t\bar{\boldsymbol{\omega}}_B \rangle$, since they cause changes in the frequency of the filter input $\boldsymbol{\Theta}\mathbf{I}_t\bar{\boldsymbol{\omega}}_B$. Sufficient time must therefore be allowed for the roll rate and bias estimates in the Kalman filter to converge before the output of the filter $G$ can be used as a measurement.

Once the secular component is isolated, pitch-over measurement construction can proceed along the original lines. Although the magnitude of the pitch-over rate can be estimated using (5.4), the main purpose of the measurement is to correct for roll angle error, not rate errors. Therefore, the filtered pitch-over rate is first changed to a unit vector.

$$\langle \boldsymbol{i}_\omega \rangle = \frac{\langle \mathbf{I}_t\bar{\boldsymbol{\omega}}_B \rangle}{|\langle \mathbf{I}_t\bar{\boldsymbol{\omega}}_B \rangle|} \tag{5.25}$$

### Vector Measurement

The measurement can now be defined as

$$\boldsymbol{z}_\gamma = \bar{\mathbf{A}}_{IB}^{\mathrm{T}}\boldsymbol{i}_{\dot{\gamma}} - \langle \boldsymbol{i}_\omega \rangle \tag{5.26}$$

Expansion of this equation should give

$$\boldsymbol{z}_\gamma = (\mathbf{I} + [\boldsymbol{\psi}_B\times])\mathbf{A}_{IB}^{\mathrm{T}}\boldsymbol{i}_{\dot{\gamma}} - \langle \boldsymbol{i}_\omega \rangle \tag{5.27}$$

However, for this measurement only roll misalignment should be allowed as an error source, since only lateral components of rate are being considered. This can be made explicit by defining the matrix $\mathbf{I}_r$ as

$$\mathbf{I}_r = \begin{bmatrix} 1 & 0 & 0 \\ 0 & 0 & 0 \\ 0 & 0 & 0 \end{bmatrix} \tag{5.28}$$

and modifying (5.27), which becomes

$$\boldsymbol{z}_\gamma = (\mathbf{I} + [(\mathbf{I}_r \boldsymbol{\psi}_B)\times])\mathbf{A}_{IB}^{\mathrm{T}} \boldsymbol{i}_{\dot{\gamma}} - \langle \boldsymbol{i}_\omega \rangle \tag{5.29}$$

Taking the partial derivative with respect to the attitude perturbation then gives

$$\mathbf{C}_{\gamma,\psi} \equiv \frac{\partial \boldsymbol{z}_\gamma}{\partial \boldsymbol{\psi}_B} = -[(\mathbf{A}_{IB}^{\mathrm{T}} i_{\dot{\gamma}})\times]\mathbf{I}_r \tag{5.30}$$

### Scalar Measurement

The difficulty with the vector form of the measurement described above is that the measurement has three components, even though only one quantity, the roll angle error, is actually being measured. This makes definition of an appropriate measurement error matrix $\mathbf{R}$ somewhat difficult. An alternative approach is to define the measurement in terms of a cross product, instead of a vector difference. Assuming that the vehicle is aligned perfectly with the velocity vector, the lateral rate vector $\langle \boldsymbol{i}_\omega \rangle$ and the projection of the gravity turn vector into the body frame $\mathbf{A}_{IB}^{\mathrm{T}} \boldsymbol{i}_{\dot{\gamma}}$ should both lie in the body y-z plane. The roll component of attitude error $\mathbf{I}_r \boldsymbol{\psi}_B$ is thus identical to the magnitude of the cross product $\mathbf{A}_{IB}^{\mathrm{T}} \boldsymbol{i}_{\dot{\gamma}} \times \langle \boldsymbol{i}_\omega \rangle$. This leads to the following alternative scalar formulation of the measurement.

Define the measurement as

$$\boldsymbol{z}_\gamma = \bar{\mathbf{A}}_{IB}^{\mathrm{T}} \boldsymbol{i}_{\dot{\gamma}} \times \langle \boldsymbol{i}_\omega \rangle \tag{5.31}$$

Since both vectors lie in (nearly) the same plane, only the x-component of the measurement is significant. Expanding:

$$\boldsymbol{z}_\gamma = [(\mathbf{I} + [(\mathbf{I}_r \boldsymbol{\psi}_B)\times])\mathbf{A}_{IB}^{\mathrm{T}} \boldsymbol{i}_{\dot{\gamma}}] \times \langle \boldsymbol{i}_\omega \rangle \tag{5.32}$$

$$\boldsymbol{z}_\gamma = (\mathbf{A}_{IB}^{\mathrm{T}} \boldsymbol{i}_{\dot{\gamma}}) \times \langle \boldsymbol{i}_\omega \rangle + [\langle \boldsymbol{i}_\omega \rangle \times][(\mathbf{A}_{IB}^{\mathrm{T}} \boldsymbol{i}_{\dot{\gamma}})\times](\mathbf{I}_r \boldsymbol{\psi}_B) \tag{5.33}$$

The partial derivative with respect to attitude perturbation is then

$$\mathbf{C}_{\gamma,\psi} \equiv \frac{\partial \boldsymbol{z}_\gamma}{\partial \boldsymbol{\psi}_B} = [\langle \boldsymbol{i}_\omega \rangle \times][(\mathbf{A}_{IB}^{\mathrm{T}} \boldsymbol{i}_{\dot{\gamma}})\times]\mathbf{I}_r \tag{5.34}$$

The vectors $\langle \boldsymbol{i}_\omega \rangle$ and $\mathbf{A}_{IB}^{\mathrm{T}} \boldsymbol{i}_{\dot{\gamma}}$ are identical within the bounds of the assumptions stated earlier, and lie entirely in the body y-z plane. The upper left hand component of $\mathbf{C}_{\gamma,\psi}$ is equal to the inner product $\langle \boldsymbol{i}_\omega \rangle^{\mathrm{T}} (\mathbf{A}_{IB}^{\mathrm{T}} \boldsymbol{i}_{\dot{\gamma}}) \approx 1$. The partial derivative matrix is therefore

$$\mathbf{C}_{\gamma,\psi} = \mathbf{I}_r \tag{5.35}$$

The scalar form of the measurement uses only the x-component of (5.31), which can be interpreted as a direct measurement of $\psi_{B_x}$, with partial derivative $\mathbf{C}_{\gamma,\psi} = 1$.

# Chapter 6

# Results

This chapter presents performance results for angular rate and roll attitude estimation under a variety of error conditions. Section 6.1 describes rate estimation performance characteristics of the filter, and gives the relationship between rate estimation error and instrument random walk, bias, misalignment, and scale factor errors. Section 6.2 describes the IIR filter used to isolate the pitch-over component of the lateral rates which was introduced in 5.3. Section 6.3 shows results for roll attitude estimation performance for varying error conditions. Throughout this chapter, accelerometer measurements were provided to the navigation filter at 100 Hz. Dynamics based vector measurements were provided to the filter at 2 Hz.

## 6.1 Rate Estimation Performance

A number of test cases were simulated to set limits on allowable random walk, bias, scale factor, and misalignment, the results of which are included in this section. Table 6.1 provides a summary of the the different test conditions for each figure shown in the section.

### 6.1.1 Unbiased Rate Estimation

Figure 6-1 shows the standard deviation of the rate estimation error predicted by the filter as a function of increasing random walk error $\sigma_{rw}$. In the test cases used to generate 6-1, no instrument biases were modelled, and the Kalman filter was configured without bias states. Quantization error was constant for all cases, with a range of $\pm 16$ g and $n = 16$. Estimates for roll and lateral rates are shown separately.

It is clear from the figure that rate estimation errors increase linearly with increasing instrument random walk for $\sigma_{rw}$ values greater than $\sim$ 0.1 milli-g/$\sqrt{\text{Hz}}$. Below this value, the rate estimation performance levels off, as the quantization component of the instrument error begins to dominate. The accuracy of the roll (x) and lateral (y and z) components of the rate differ slightly, reflecting the superior signal strength available for roll estimation due to vehicle spin rate.

Table 6.1: Rate estimation results summary

| Figure | $\sigma_{rw}$ | Bias | Scale Factor | Misalign-ment | EKF Comp. | Process Noise | Rate Rate |
|---|---|---|---|---|---|---|---|
| 6-1 | Varies | 0 | 0 | 0 | Yes | 0 | Both |
| 6-2 | 0.5 | 250 | 0 | 0 | No | 0 | Both |
| 6-3 | 0.5 | 250 | 0 | 0 | Yes | 0 | Both |
| 6-4 | 0.5 | Varies | 0 | 0 | No | 0 | Roll |
| 6-5 | 0.5 | Varies | 0 | 0 | Partial | 0 | Roll |
| 6-6 | 0.5 | Varies | 0 | 0 | Yes | 0 | Roll |
| 6-7 | Varies | 500 | 0 | 0 | Yes | 0 | Roll |
| 6-8 | Varies | 500 | 0 | 0 | Yes | 0 | Lateral |
| 6-9 | 1 | Varies | 0 | 0 | Yes | 0 | Roll |
| 6-10 | 1 | Varies | 0 | 0 | Yes | 0 | Lateral |
| 6-11 | 2.5 | Varies | 0 | 0 | Yes | 0 | Roll |
| 6-12 | 2.5 | Varies | 0 | 0 | Yes | 0 | Lateral |
| 6-13 | 0.5 | 500 | Varies | 0 | Yes | 0 | Roll |
| 6-14 | 0.5 | 500 | Varies | 0 | Yes | 0 | Lateral |
| 6-15 | 0.5 | 500 | 0 | Varies | Yes | 0 | Roll |
| 6-16 | 0.5 | 500 | 0 | Varies | Yes | 0 | Lateral |
| 6-17 | 0.5 | 500 | 0 | Varies | Yes | 50 | Roll |
| 6-18 | 0.5 | 500 | 0 | Varies | Yes | 50 | Lateral |

### 6.1.2 Rate Estimation with Biases

As noted in Section 4.5, rate estimation in the presence of large biases is more difficult. Without the modifications to the extended Kalman filter described in that section, severe rate estimate divergence was common, as in Figure 6-2. Performance was significantly improved using the EKF compensation techniques outlined in 4.5. Figure 6-3 was generated using the same data set as Figure 6-2, but with the EKF compensation technique enabled. The particular case shown used values of $\sigma_{rw} = 0.5$ milli-g/$\sqrt{\text{Hz}}$, with 250 milli-g RMS bias, but the enormous improvement in convergence shown in the example held for nearly all cases tested.

As expected, the probability of filter divergence increased for larger initial instrument biases. Figure 6-4 clearly shows a large divergence in the roll rate estimation error for initial RMS bias values greater than about 250 milli-g, using an instrument random walk value of 0.5 milli-g/$\sqrt{\text{Hz}}$. The effect of enabling EKF compensation, but *without* setting a minimum value of $\sigma_{rw}$, is demonstrated in Figure 6-5. It is clear that linearization compensation makes a major improvement in performance, as well as allowing for somewhat more graceful failure on the part of the estimator as errors increase. The results are still far from perfect however, which is a side effect of the very low noise in the sensors. The improvement gained from setting a minimum value for $\sigma_{rw}$ is evident from Figure 6-6.

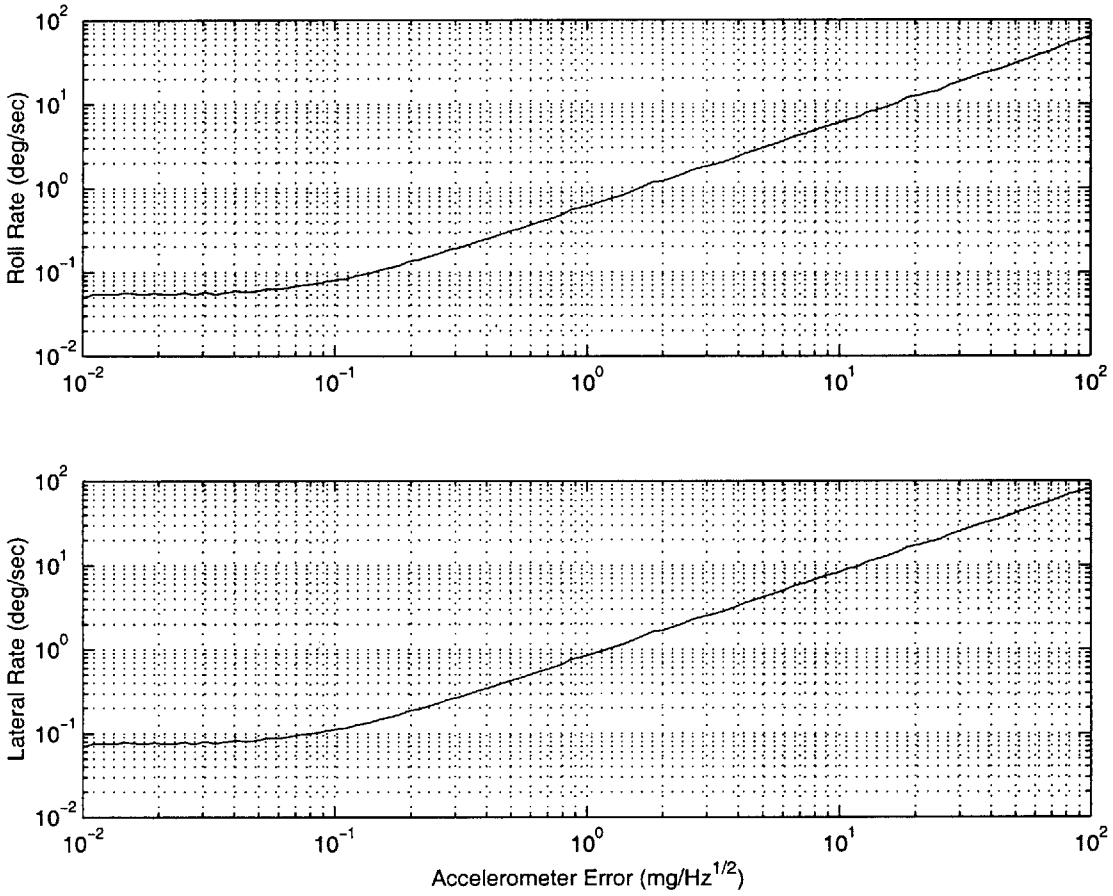


Figure 6-1: Steady state rate estimation error vs accelerometer random walk $\sigma_{rw}$ - no bias states or errors.

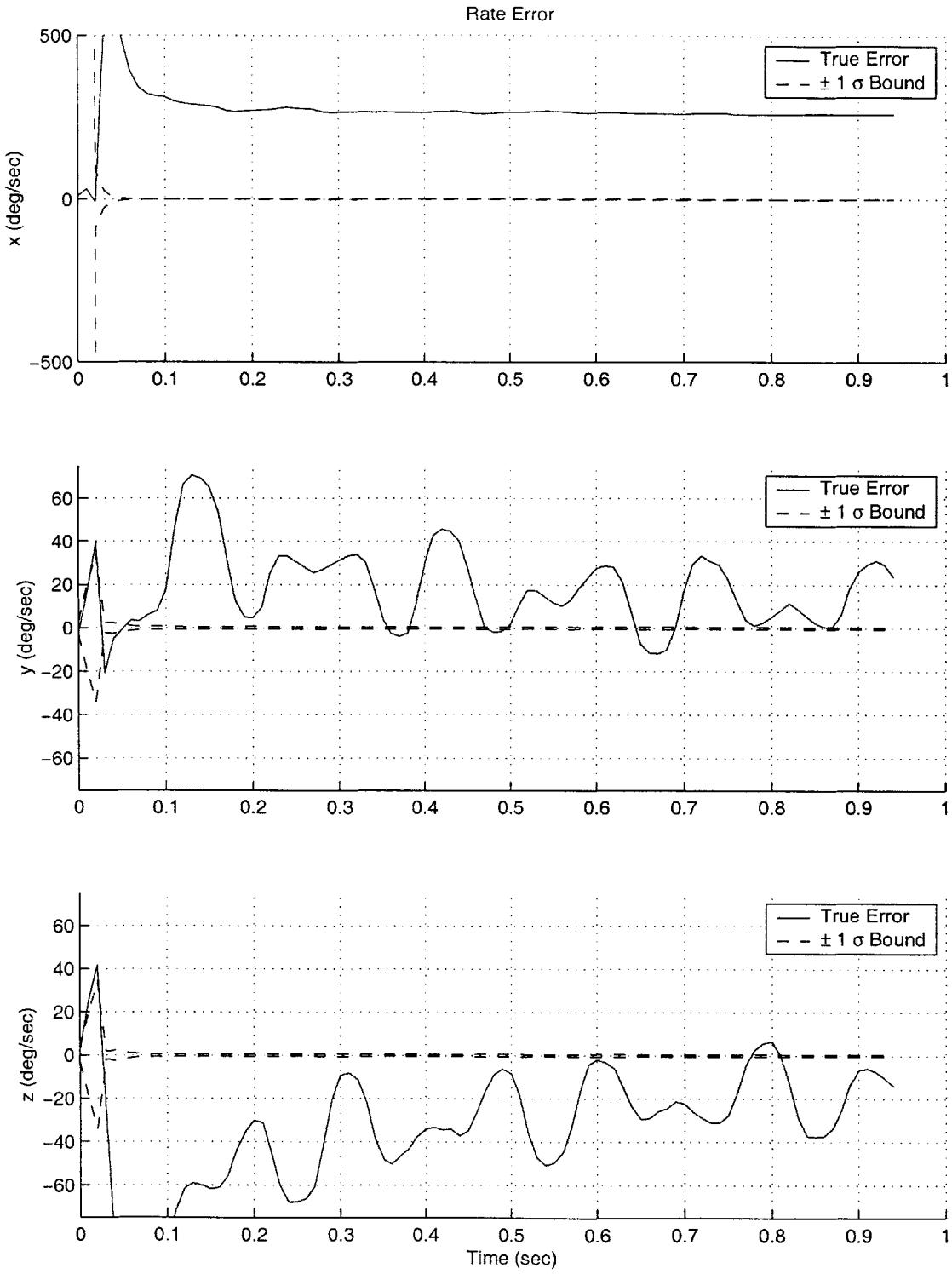


Figure 6-2: Example - Rate estimation divergence due to uncompensated filter linearization errors at initialization. (250 milli-g RMS bias, $\sigma_{rw} = 0.5$ milli-g/$\sqrt{\text{Hz}}$)

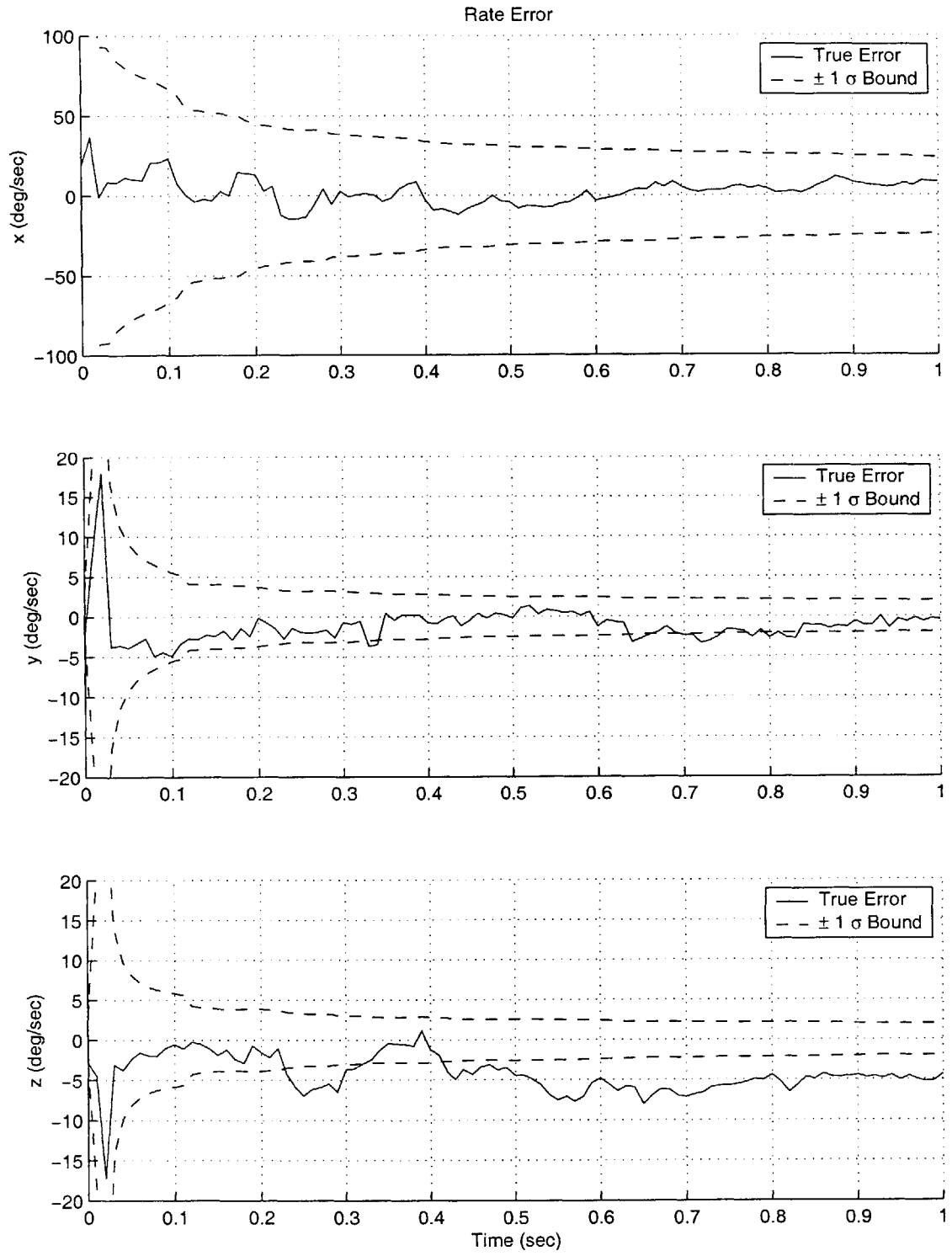


Figure 6-3: Example - Rate estimation convergence using EKF compensation technique of Section 4.5. (250 milli-g RMS bias, $\sigma_{rw} = 0.5$ milli-g/$\sqrt{\text{Hz}}$ )

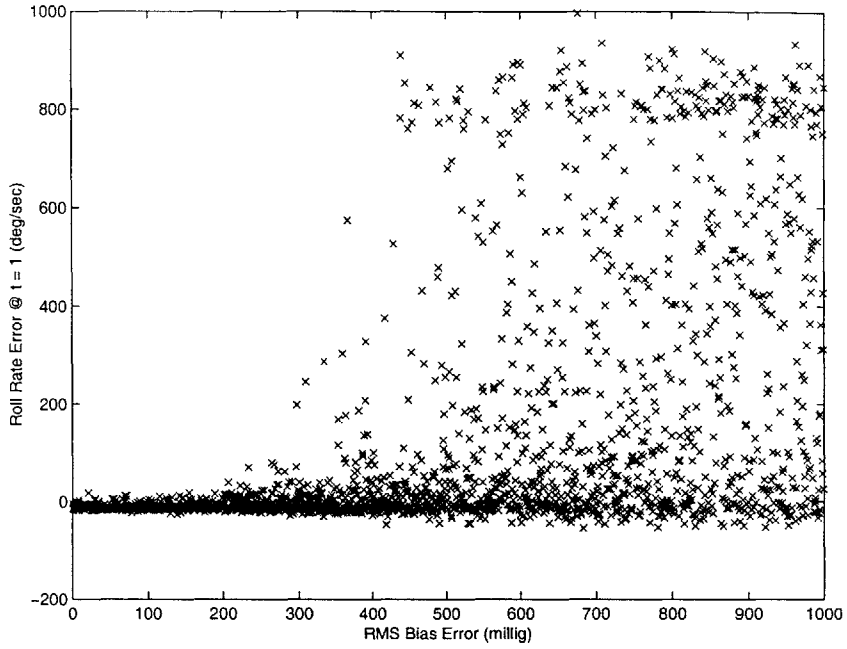


Figure 6-4: Roll rate estimation error at $t = 1$ sec vs bias *without* EKF compensation technique of Section 4.5. Large errors above 500 milli-g RMS bias are due to uncompensated linearization errors during filter initialization. ($\sigma_{rw} = 0.5$ milli-g/$\sqrt{\text{Hz}}$)

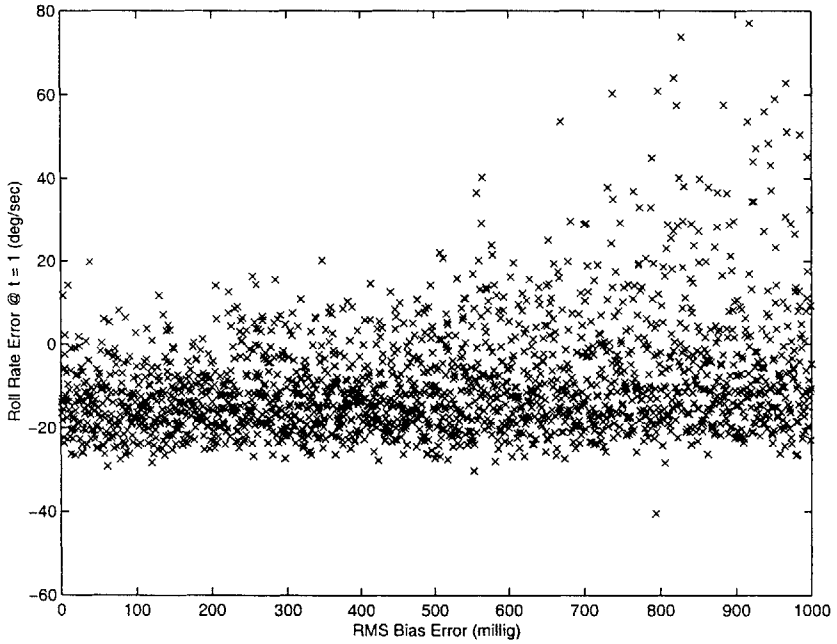


Figure 6-5: Roll rate estimation error at $t = 1$ sec vs bias *with* EKF compensation technique of Section 4.5. Rate estimation error above 200 milli-g RMS bias is significantly improved. Increased error above 500 milli-g RMS bias is caused by very small $\sigma_{rw}$ value in navigation filter. ($\sigma_{rw} = 0.5$ milli-g/$\sqrt{\text{Hz}}$)

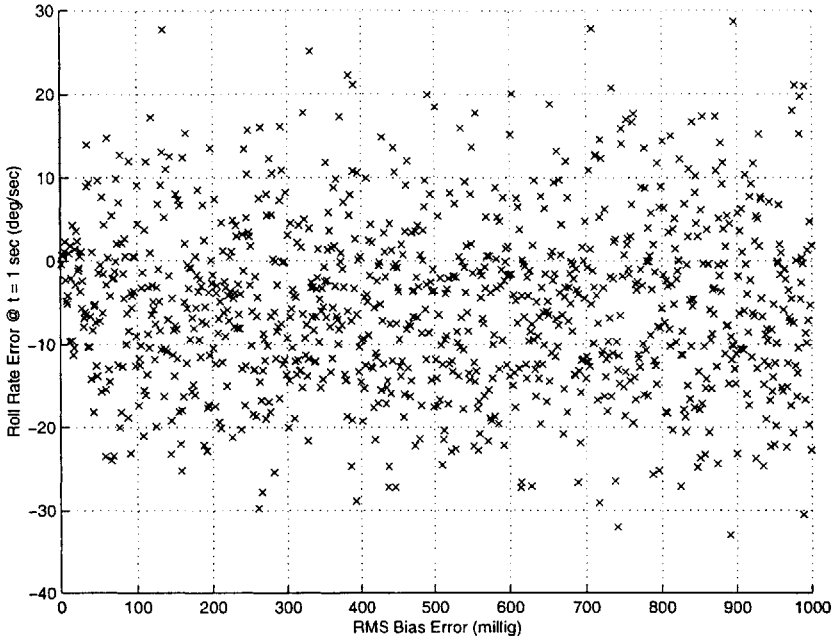


Figure 6-6: Roll rate estimation error at $t = 1$ sec vs bias *with* EKF compensation technique of Section 4.5. Further reduction in rate estimation error is achieved by setting a lower bound ($\sigma_{rw} = 1.5$ milli-g/$\sqrt{\text{Hz}}$) in the navigation filter. ($\sigma_{rw} = 0.5$ milli-g/$\sqrt{\text{Hz}}$)

For the complete set of EKF corrections, *including* a lower bound of 1.5 milli-g/$\sqrt{\text{Hz}}$ for $\sigma_{rw}$, rate estimation showed very strong convergence over the full range of RMS bias values tested (0–1000 milli-g RMS bias), and for the range of $\sigma_{rw}$ value tested (0.5–10 milli-g/$\sqrt{\text{Hz}}$), with no apparent decrease in convergence rate for large biases.

The effect of increasing random walk error over 1000 test cases is shown in Figures 6-7 and 6-8. Results for varying levels of instrument bias for different constant values of $\sigma_{rw}$ are included as Figures 6-9 – 6-12.

These plots collectively show that, as expected, rate estimation performance is strongly tied to instrument random walk error. Bias error seems to have little or no impact in rate estimation performance, at least within the range tested. It should also be noted that in some cases, particularly for low noise levels, the rate estimate has a systematic error of ~8 deg. The source of this error is not known. It is not of major concern however, as it tends to disappear when the dynamics-based methods of Chapter 5 are introduced.

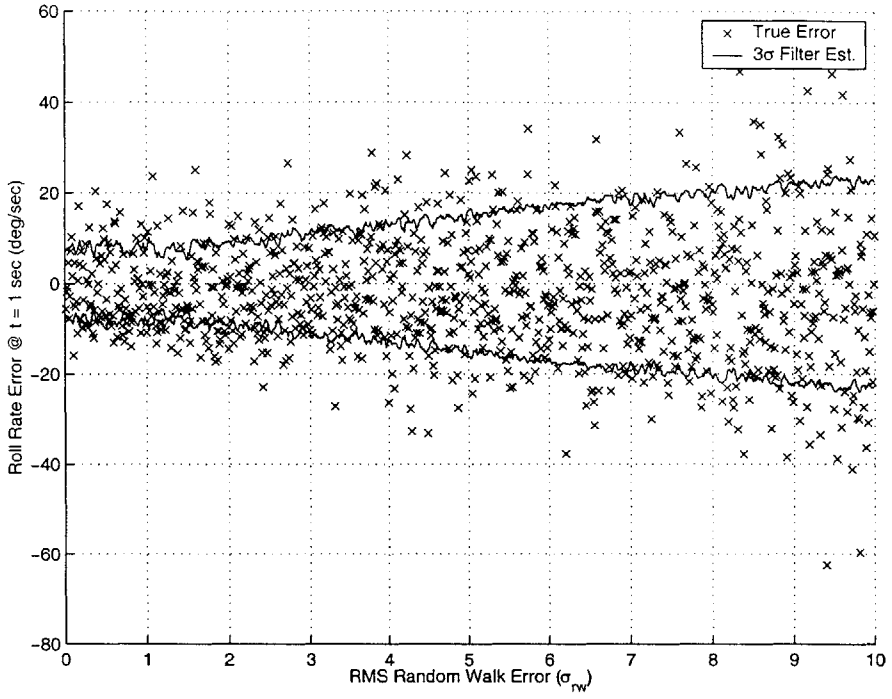


Figure 6-7: Roll rate estimation error vs $\sigma_{rw}$ at $t = 1$ sec. (500 milli-g RMS bias)

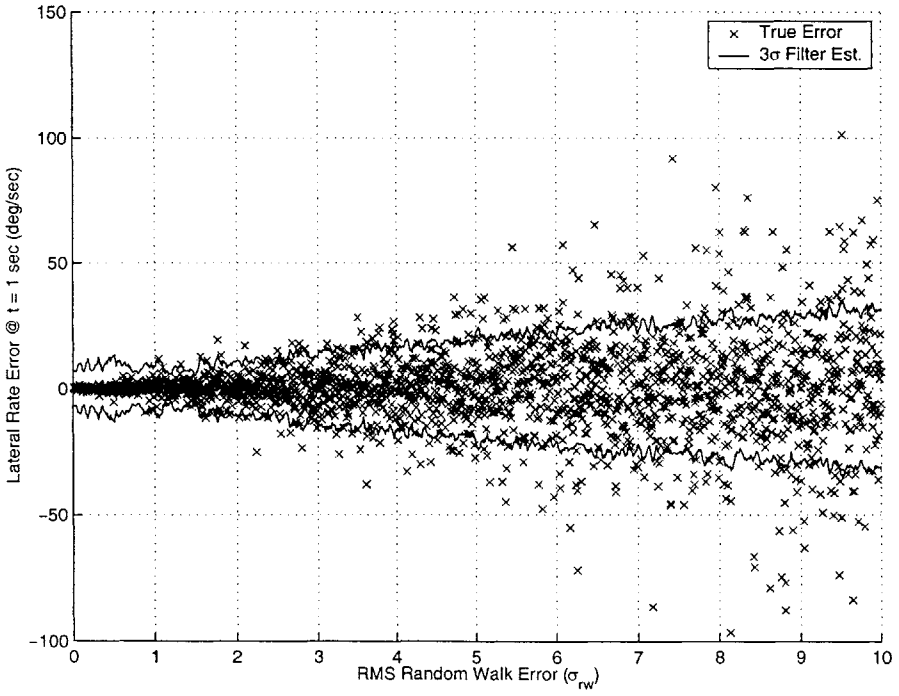


Figure 6-8: Lateral rate estimation error vs $\sigma_{rw}$ at $t = 1$ sec. (500 milli-g RMS bias)

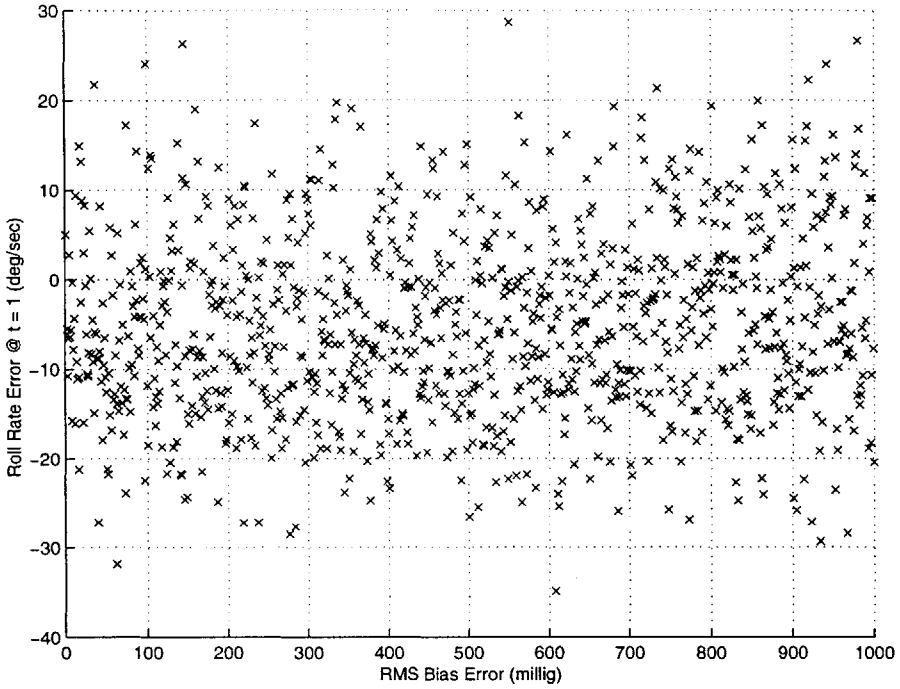


Figure 6-9: Roll rate estimation error vs RMS bias at $t = 1$ sec. ($\sigma_{rw} = 1$ milli-g/$\sqrt{\text{Hz}}$)

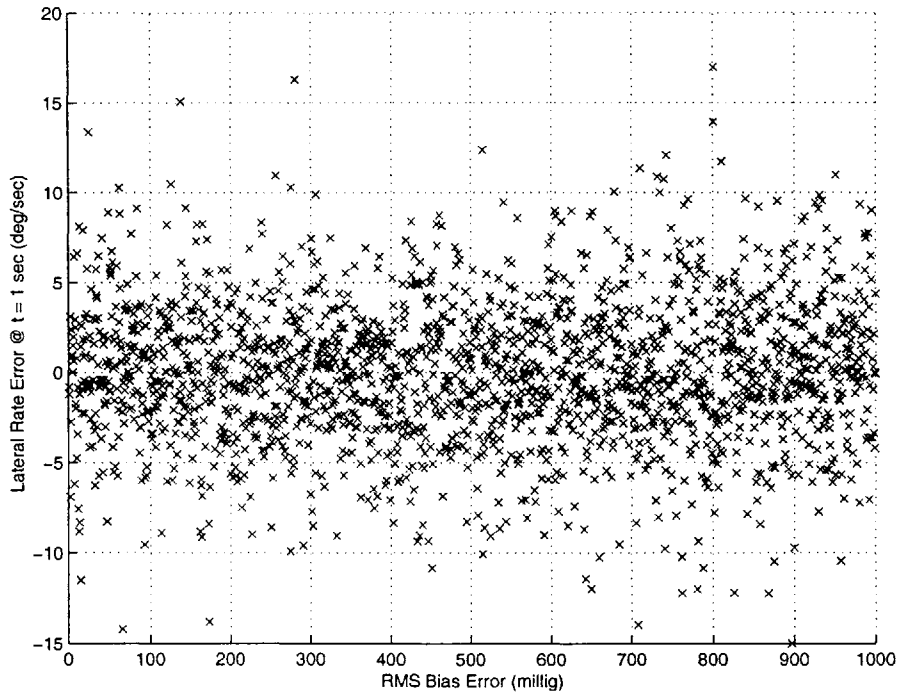


Figure 6-10: Lateral rate estimation error vs RMS bias at $t = 1$ sec. ($\sigma_{rw} = 1$ milli-g/$\sqrt{\text{Hz}}$)

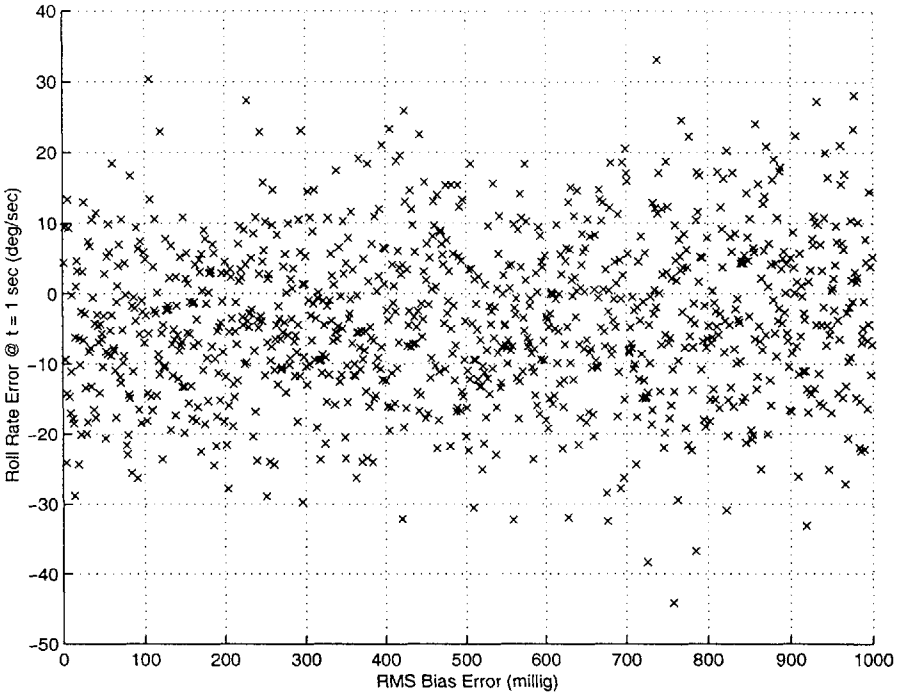


Figure 6-11: Roll rate estimation error vs RMS bias at $t = 1$ sec. ($\sigma_{rw} = 5$ milli-g/$\sqrt{\text{Hz}}$)

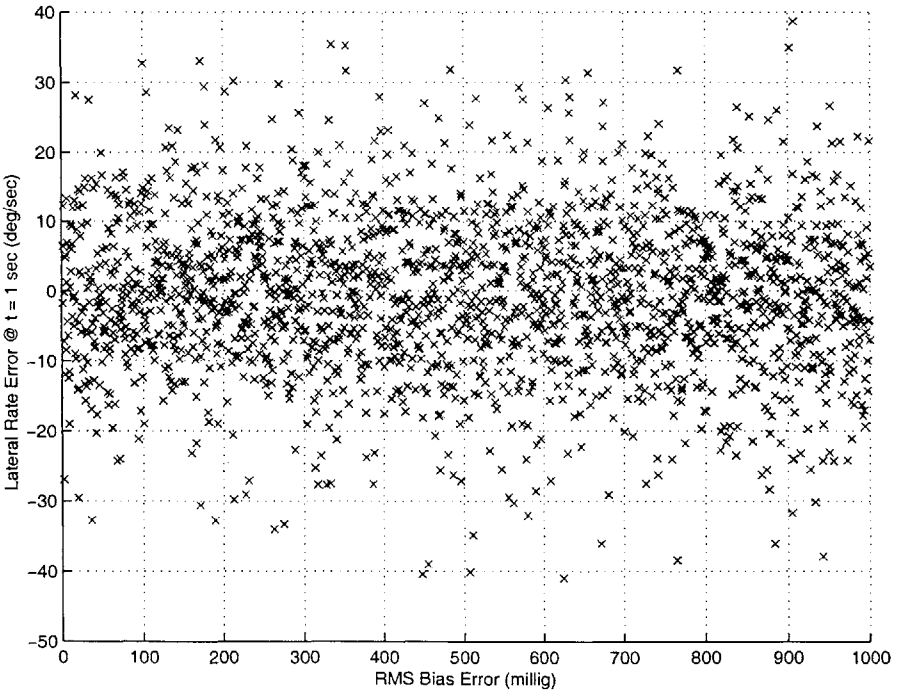


Figure 6-12: Lateral rate estimation error vs RMS bias at $t = 1$ sec. ($\sigma_{rw} = 5$ milli-g/$\sqrt{\text{Hz}}$)

### 6.1.3 Rate Estimation with Scale Factor and Misalignment Errors

No states were included in the filter to explicitly handle accelerometer misalignments and scale factor errors. However, as noted in Section 4.2.6, these types of errors can be partially compensated for through bias estimation.

Two tests were conducted to characterize filter performance for increasing misalignments and scale factor errors. Accelerometer $\sigma_{rw}$ values of 0.5 milli-g/$\sqrt{\text{Hz}}$ and RMS bias errors of 500 milli-g were used in both cases.

For the scale factor test, roll rate estimation performance was quite good over the entire range of scale factors tested (up to 5000 ppm), and lateral rate estimation performance was unaffected up to about 2000 ppm. For larger scale factor errors, large estimation errors can be seen in a small number of cases, although performance remained quite good in the majority.

Filter performance with sensor misalignments was somewhat less impressive. Rate estimation fared badly for RMS misalignment values greater than about 0.2 deg, as shown in Figures 6-15–6-16. This was partly fixed through the addition of a process noise of $\boldsymbol{\nu}_\beta$ of 50 milli-g/$\sqrt{\text{Hz}}$ in the navigation filter. This helped to alleviate the errors caused by time varying drag force, which are seen by the misaligned sensors as a time-varying error. This technique improved rate estimation substantially, as shown in Figures 6-17–6-16, and allowed for reliable rate estimation through about 1 degree misalignment error, with relatively graceful degradation thereafter.

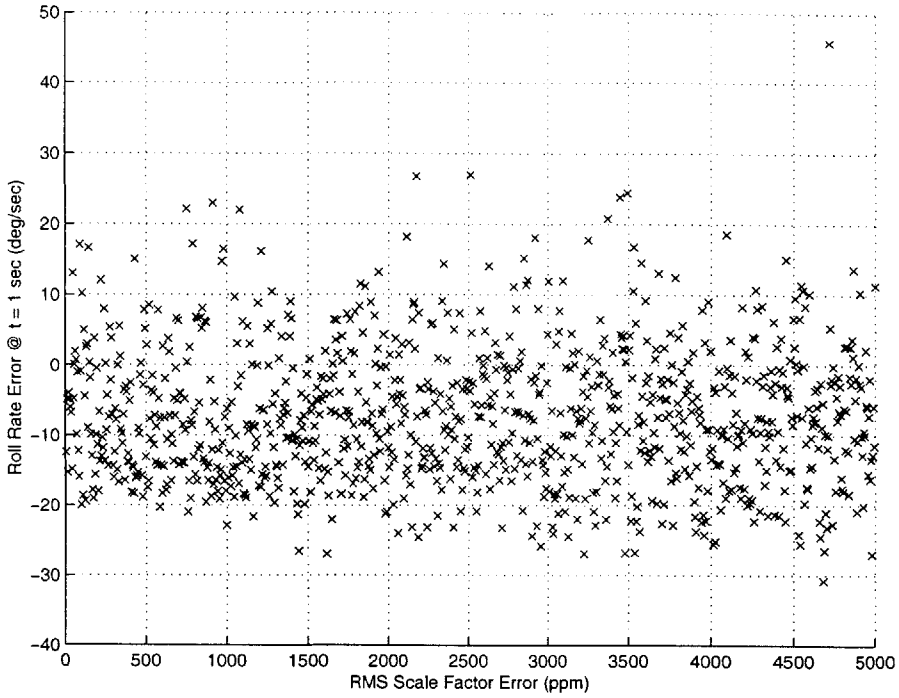


Figure 6-13: Roll rate estimation error vs scale factor error (ppm) at $t = 1$ sec. ($\sigma_{rw} = 0.5$ milli-g/$\sqrt{\text{Hz}}$, RMS bias = 500 milli-g/$\sqrt{\text{Hz}}$ )

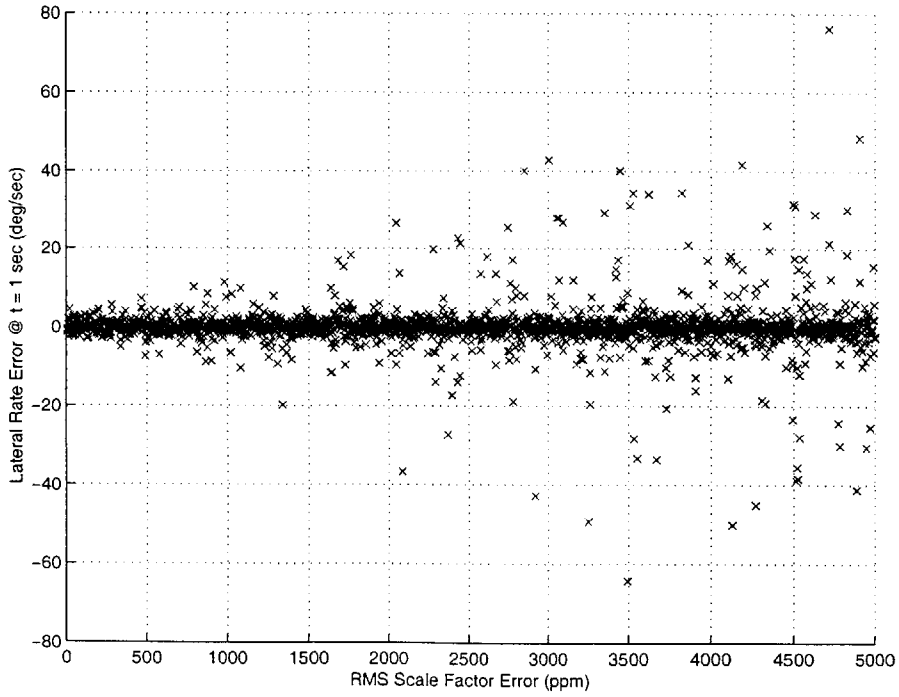


Figure 6-14: Lateral rate estimation error vs scale factor error (ppm) at $t = 1$ sec. ($\sigma_{rw} = 0.5$ milli-g/$\sqrt{\text{Hz}}$, RMS bias = 500 milli-g/$\sqrt{\text{Hz}}$ )

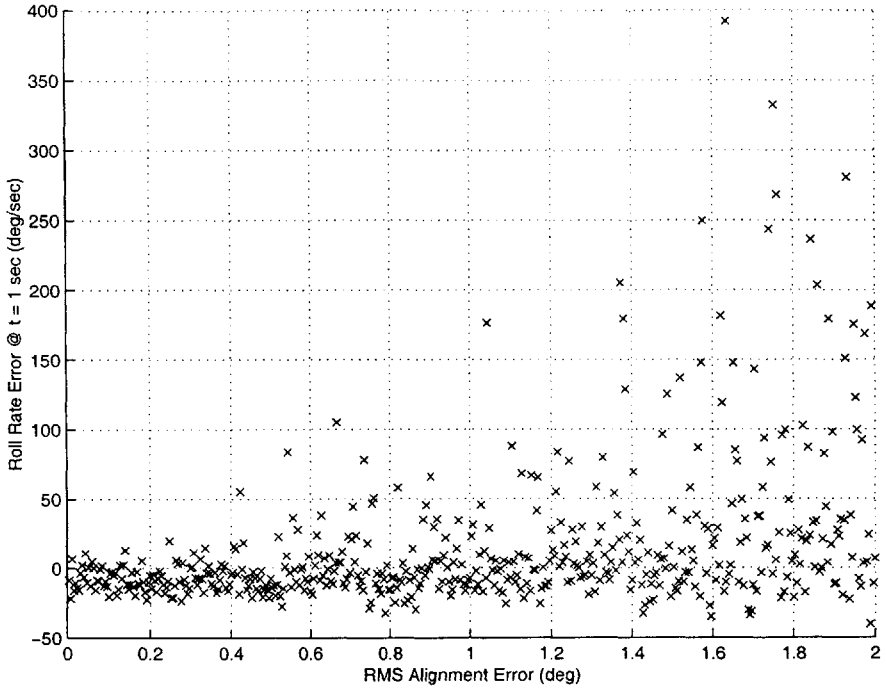


Figure 6-15: Roll rate estimation error vs sensor misalignment error at $t = 1$ sec, no bias state process noise. ($\sigma_{rw} = 0.5$ milli-g/$\sqrt{\text{Hz}}$, RMS bias = 500 milli-g/$\sqrt{\text{Hz}}$ )

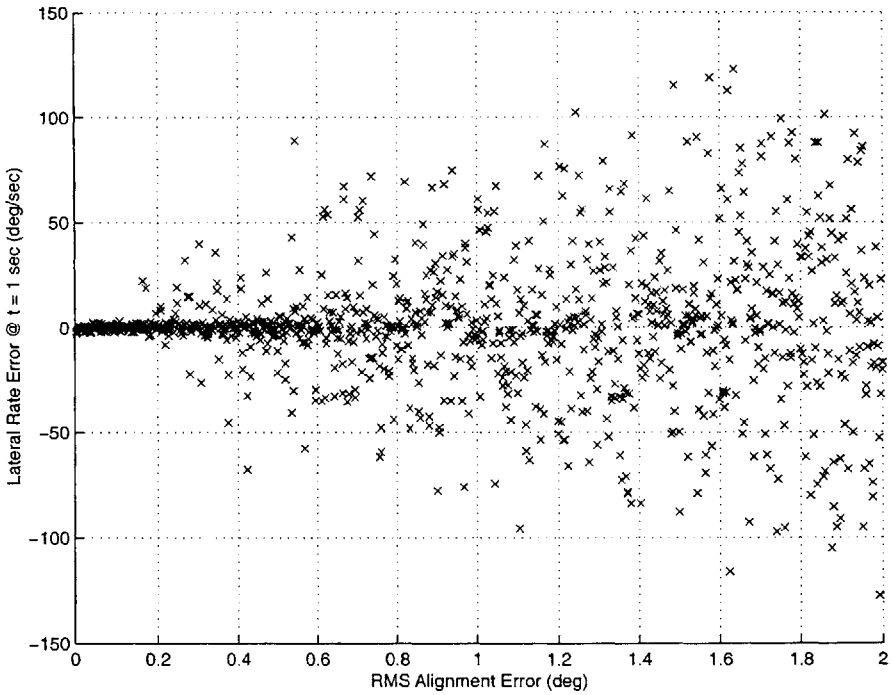


Figure 6-16: Lateral rate estimation error vs sensor misalignment error at $t = 1$ sec, no bias state process noise. ($\sigma_{rw} = 0.5$ milli-g/$\sqrt{\text{Hz}}$, RMS bias = 500 milli-g/$\sqrt{\text{Hz}}$ )

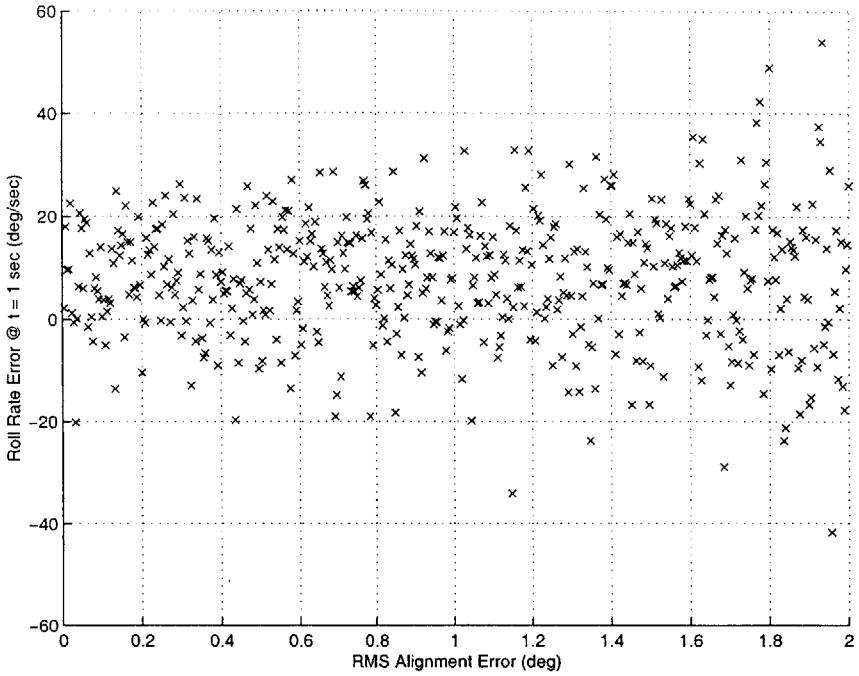


Figure 6-17: Roll rate estimation error vs sensor misalignment error at $t = 1$ sec, bias state process noise = 50 milli-g/$\sqrt{\text{Hz}}$. ($\sigma_{rw} = 0.5$ milli-g/$\sqrt{\text{Hz}}$, RMS bias = 500 milli-g/$\sqrt{\text{Hz}}$ )

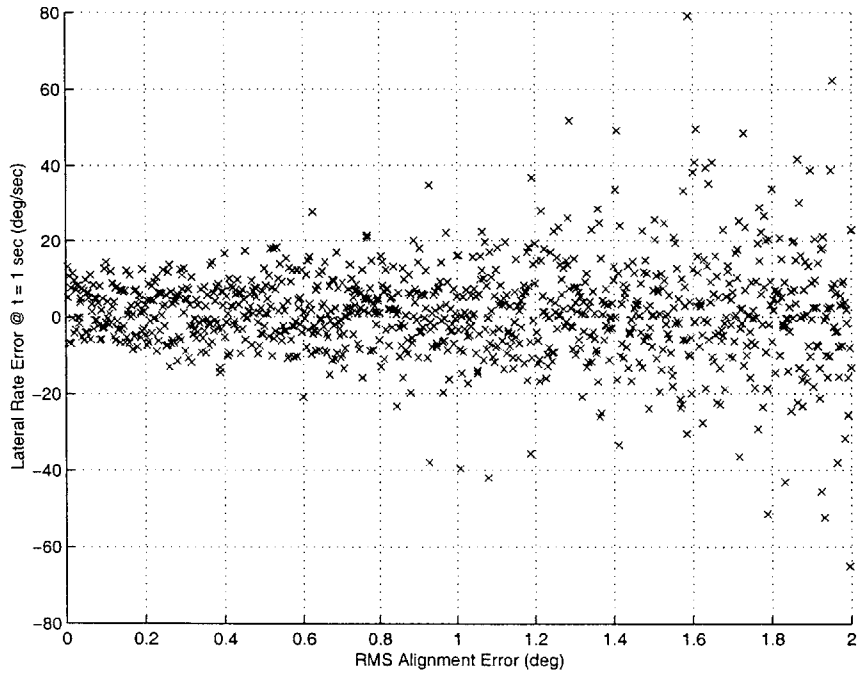


Figure 6-18: Lateral rate estimation error vs sensor misalignment error at $t = 1$ sec, bias state process noise = 50 milli-g/$\sqrt{\text{Hz}}$. ($\sigma_{rw} = 0.5$ milli-g/$\sqrt{\text{Hz}}$, RMS bias = 500 milli-g/$\sqrt{\text{Hz}}$ )

## 6.2 IIR Filter Design

### 6.2.1 Lateral Rate Frequency Content

Isolation of the secular pitch-over component of the lateral rate first requires an understanding of the frequency-domain characteristics of the lateral rate signal. Figure 6-19 shows the power spectral density (PSD) of the *true* lateral rate[1] in the intermediate, non-rolling frame introduced in Section 5.3.1. Of particular interest in this figure is the large spike that occurs around 4 Hz, which corresponds to the resonant pitching frequency of the shell, and is many times larger than the secular (0 Hz) component of the PSD. The size of the peak is proportional to the maximum angle of attack of the projectile. The PSD of the figure corresponds to about 1.5 deg precession amplitude.

Increasing noise levels causes the PSD of the *estimated* lateral rate to diverge somewhat from that of the true signal. Figure 6-20 shows the effect of increasing levels of accelerometer random walk error $\sigma_{rw}$ on the PSD over the frequency range of interest. The PSD of the lateral rate shows a near-uniform increase in power level with increasing noise, which serves to obscure the true rate signal.

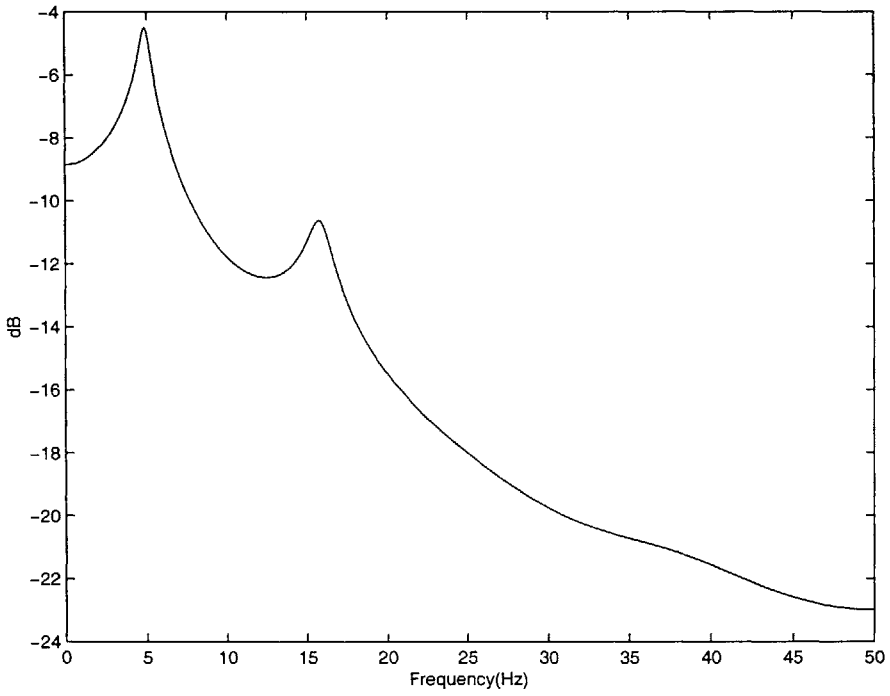


Figure 6-19: Power spectral density of true lateral rate in the non-rolling frame. Pitch-over contribution of lateral rates is the 0 Hz component of the signal. Peak at 4 Hz is resonant pitching frequency of the projectile.

[1]This figure shows power spectral density between 0 and 10 seconds after launch. The resonant pitching frequency then decreases with decreasing atmospheric density.

### 6.2.2 Filter Specifications

Based on the frequency content of the lateral rate signal, an 8th order, Butterworth low-pass IIR filter was designed using Matlab. The cutoff frequency for the filter was set to 2 Hz, or approximately 1/2 of the precession frequency. The value was chosen based the need to effectively isolate the pitch-over signal while maintaining a reasonably short settling time for the filter. Bode plots and step response for the filter implemented are shown in Figure 6-21.

### 6.2.3 Filter Performance

IIR performance can be evaluated based on the definition of the gravity-turn pseudo-measurement $\langle \boldsymbol{i}_\omega \rangle$ defined in Section 5.3.1. The error in the IIR filter output can be taken as the angle between the estimated pitch-over vector $\langle \boldsymbol{i}_\omega \rangle$, and the true pitch-over direction $\mathbf{A}_{IB}^{\mathrm{T}} \boldsymbol{i}_{\dot{\gamma}}$. Figure 6-22 shows the behavior of this signal for a low sensor noise case. The IIR measurement takes approximately 7 seconds to converge, and settles to less than 5 degrees measurement error.

It is important to remember that this signal represents the error in the normalized low-pass filter output $\langle \boldsymbol{i}_\omega \rangle$, and *not* the roll error in the navigation filter. The signal in 5.3.1 is clearly correlated and non-Gaussian, although it is treated as uncorrelated and Gaussian by the navigation filter. This requires a somewhat arbitrary estimate

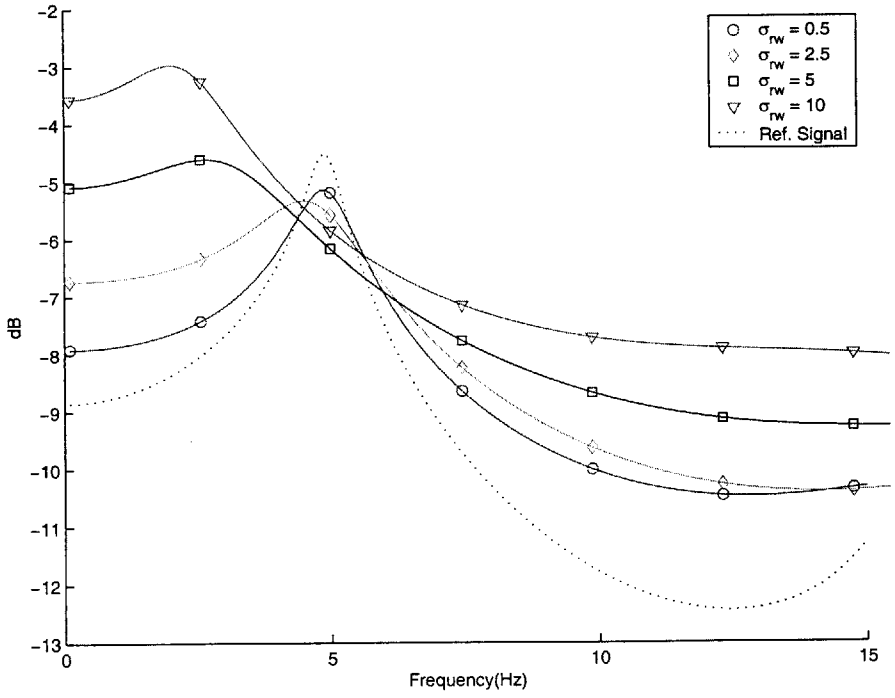


Figure 6-20: Power spectral density of lateral rate estimate in the estimated non-rolling frame. Constant component due to projectile pitch-over becomes obscured by larger values of $\sigma_{rw}$. PSD of true signal is shown for reference.

of the measurement noise to be made. In the navigation filter, measurement noise for the signal was taken to have a standard deviation equal to the maximum roll measurement error after 10 seconds. Figure 6-23 shows the same signal over the time interval 10-20 seconds, for increasing levels of random walk error. The large measurement errors seen in the figure are a direct result of the increasing noise levels also seen in Figure 6-20.

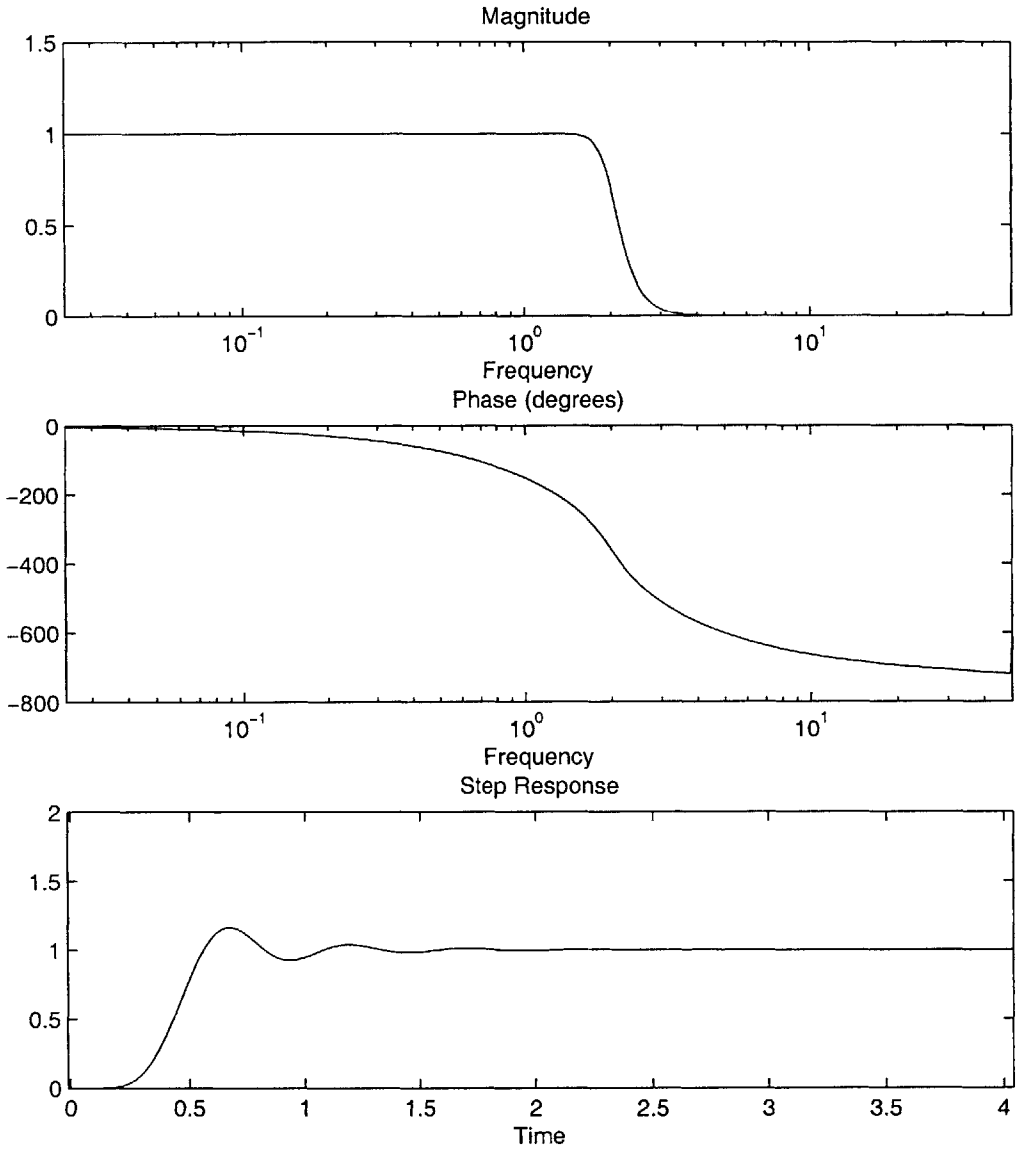


Figure 6-21: IIR filter design. Frequency response characteristics for $8^{th}$ order Butterworth IIR filter used to isolate pitch-over component of lateral rate. Cutoff frequency is 2 Hz.

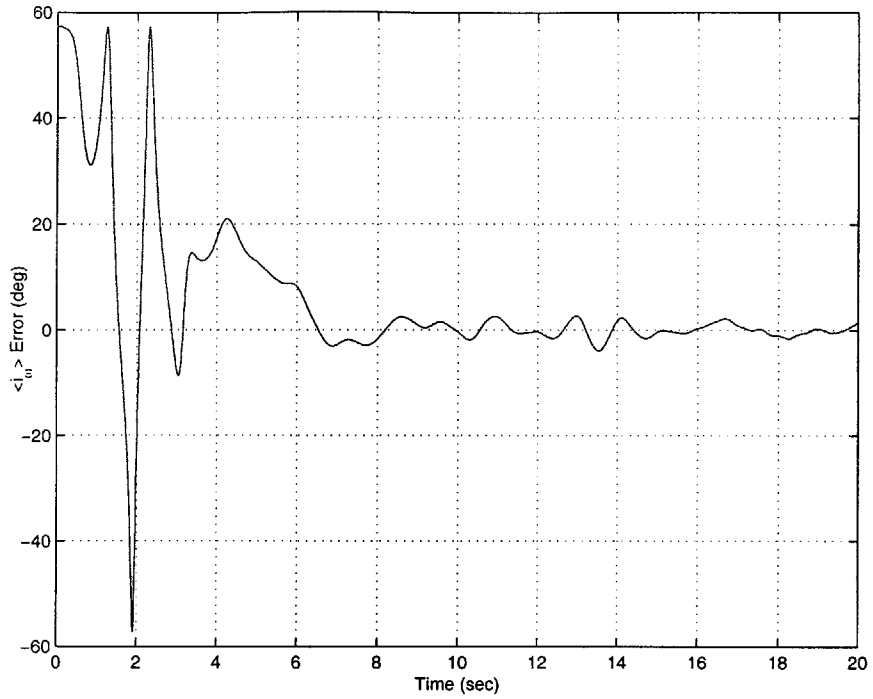


Figure 6-22: Gravity-turn vector $\langle \boldsymbol{i}_\omega \rangle$ error convergence. This signal is used in the Kalman navigation filter after the output of the IIR filter converges to a steady state at $t \sim 7$ sec. ($\sigma_{rw} = 0.5$ milli-g/$\sqrt{\text{Hz}}$)

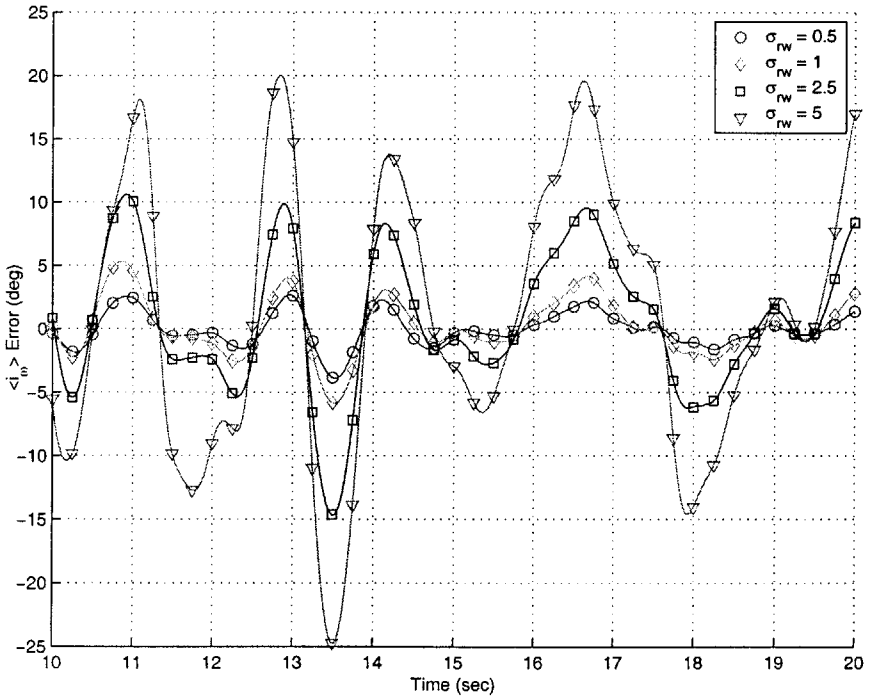


Figure 6-23: Steady-state gravity-turn vector $\langle \boldsymbol{i}_\omega \rangle$ error for different levels of $\sigma_{rw}$. Measurement standard deviation in the navigation filter is taken to be the maximum $\langle \boldsymbol{i}_\omega \rangle$ error after 10 sec.

## 6.3 Attitude Estimation Performance

Attitude estimation performance was tested for 4 different values of accelerometer random walk error $\sigma_{rw}$, with 250 test cases for each value. Accelerometer RMS bias was 500 milli-g in each case. Estimation error for the pitch-over pseudo-measurement in each case was based on the results presented and discussed in Section 6.2.3. Estimation error for the velocity alignment pseudo-measurement was based on the angle of attack of the projectile, and was fixed at 1 degree.

Figures 6-24–6-31 show the roll attitude estimation error in the navigation filter after 20 seconds of flight time for each configuration listed in Table 6.2. The top figure in each pair shows the relationship between initial and final attitude estimation error, while the bottom gives a histogram of final roll estimation error.

Table 6.2: Roll attitude estimation results summary

| Figure | $\sigma_{rw}$ | Bias | Plot Type |
|---|---|---|---|
| 6-24 | 0.5 | 500 | vs Initial Roll Error |
| 6-25 | 0.5 | 500 | Histogram |
| 6-26 | 1 | 500 | vs Initial Roll Error |
| 6-27 | 1 | 500 | Histogram |
| 6-28 | 2.5 | 500 | vs Initial Roll Error |
| 6-29 | 2.5 | 500 | Histogram |
| 6-30 | 5 | 500 | vs Initial Roll Error |
| 6-31 | 5 | 500 | Histogram |

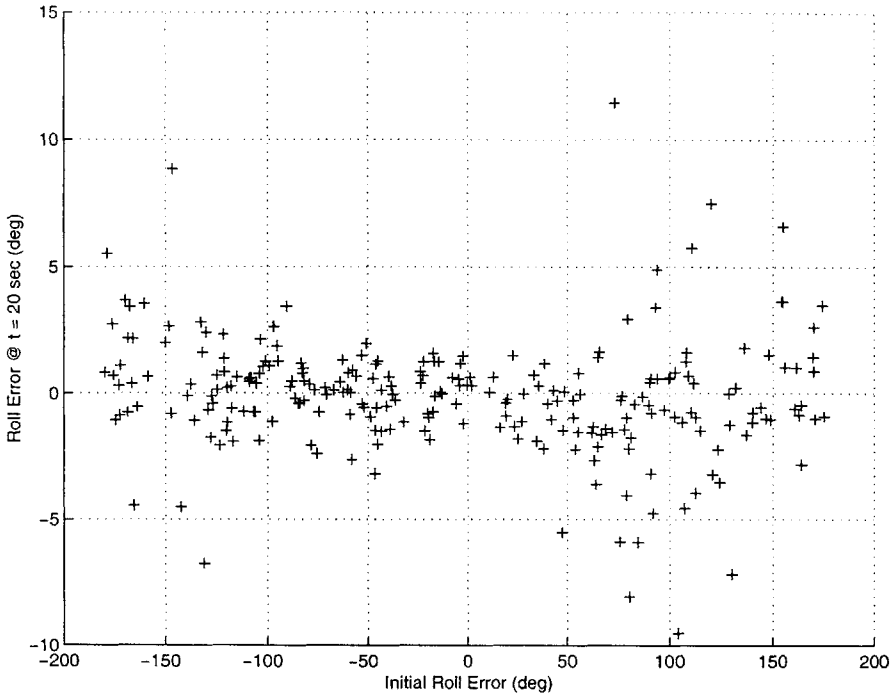


Figure 6-24: Roll angle estimation error vs initial error. ($\sigma_{rw} = 0.5$ milli-g/$\sqrt{\text{Hz}}$)

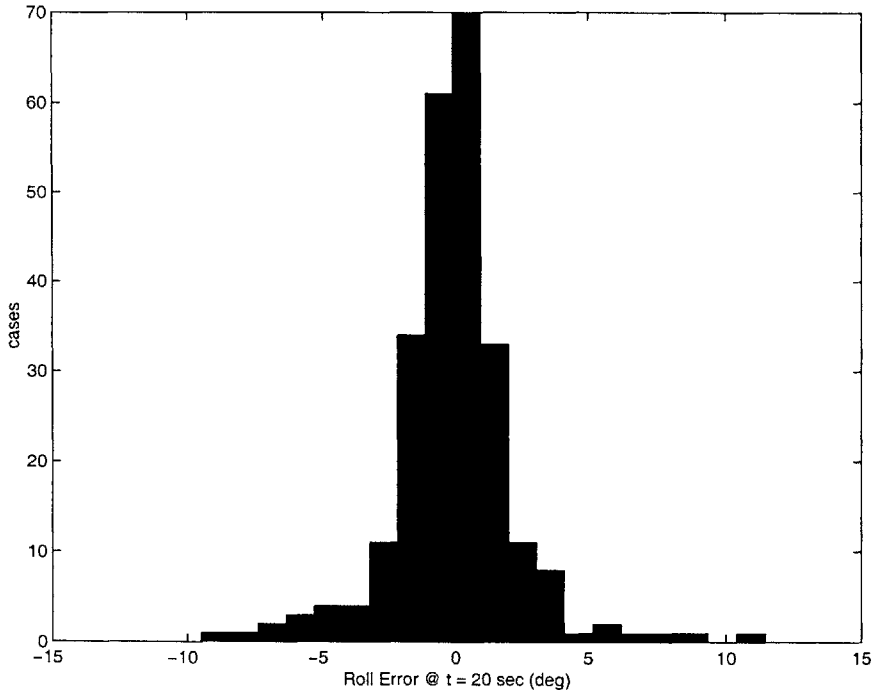


Figure 6-25: Roll angle estimation error distribution. ($\sigma_{rw} = 0.5$ milli-g/$\sqrt{\text{Hz}}$)

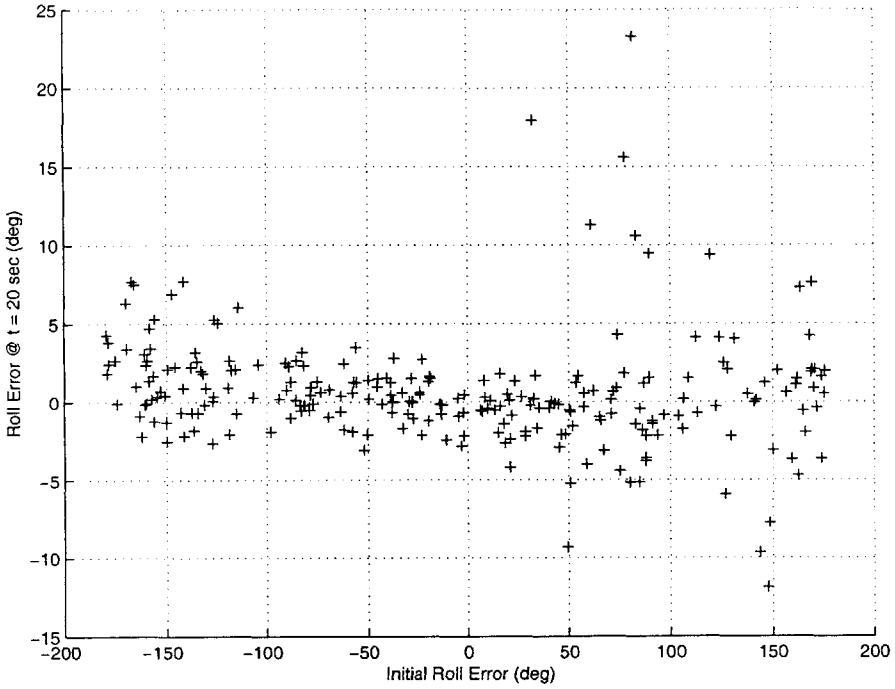


Figure 6-26: Roll angle estimation error vs initial error. ($\sigma_{rw} = 1$ milli-g/$\sqrt{\text{Hz}}$)

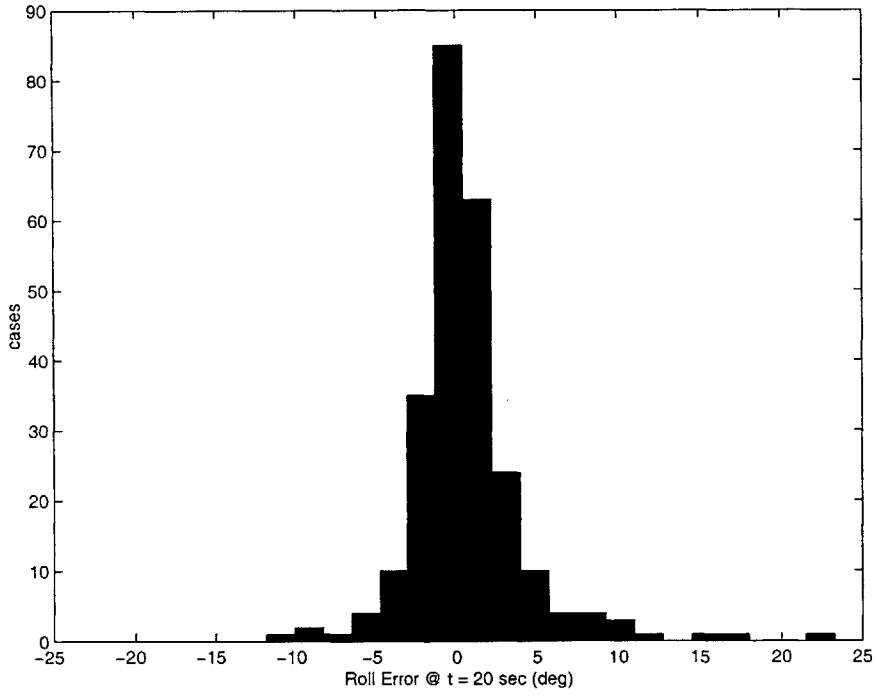


Figure 6-27: Roll angle estimation error distribution. ($\sigma_{rw} = 1$ milli-g/$\sqrt{\text{Hz}}$)

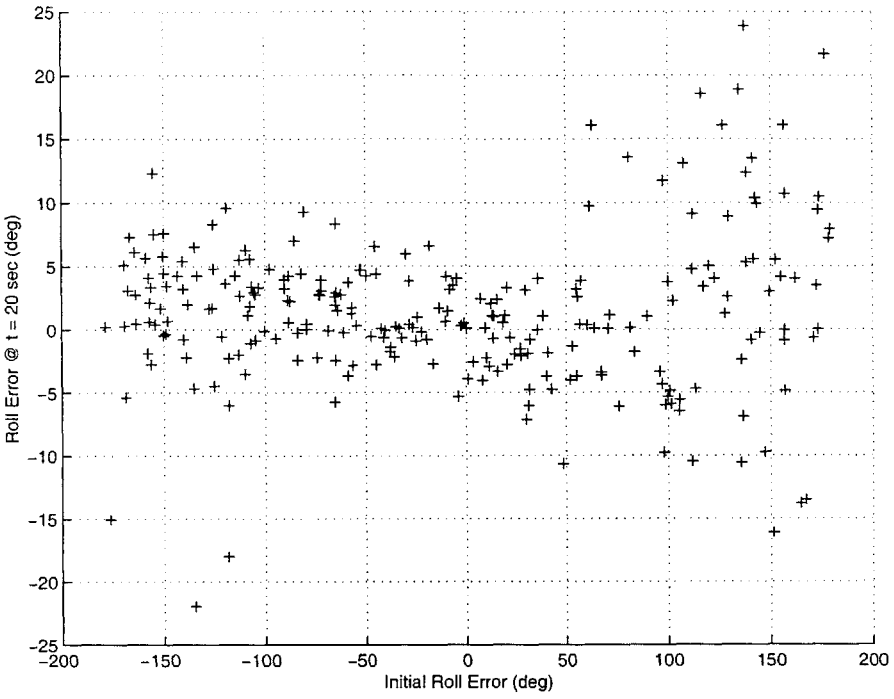


Figure 6-28: Roll angle estimation error vs initial error. ($\sigma_{rw} = 2.5$ milli-g/$\sqrt{\text{Hz}}$)

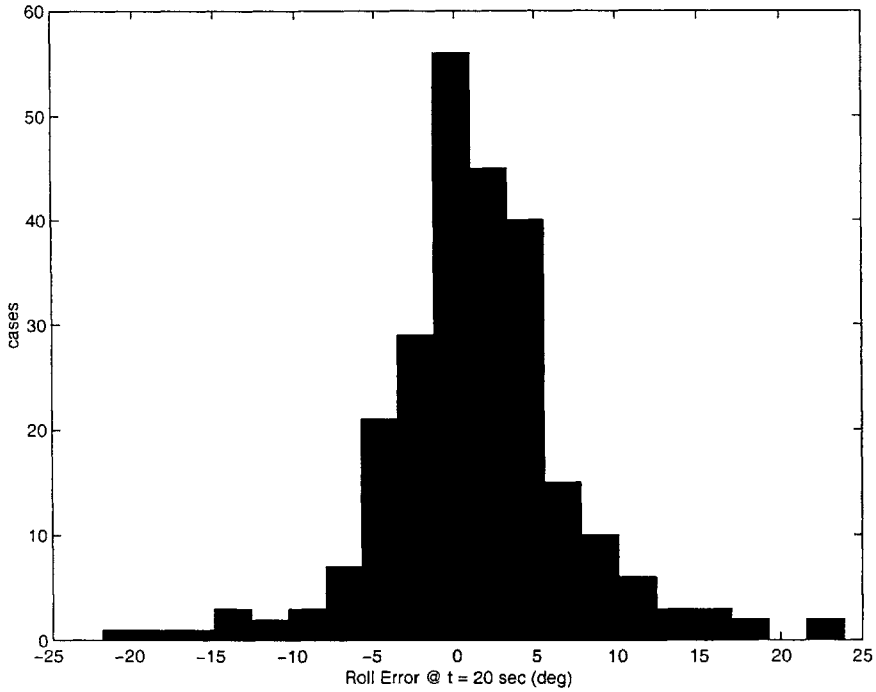


Figure 6-29: Roll angle estimation error distribution. ($\sigma_{rw} = 2.5$ milli-g/$\sqrt{\text{Hz}}$)

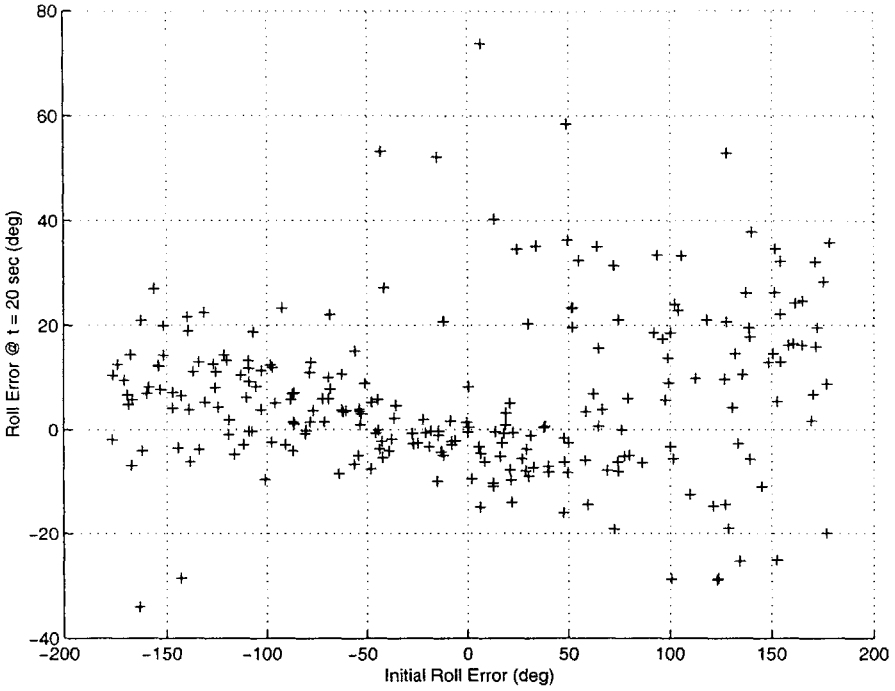


Figure 6-30: Roll angle estimation error vs initial error. ($\sigma_{rw} = 5$ milli-g/$\sqrt{\text{Hz}}$)

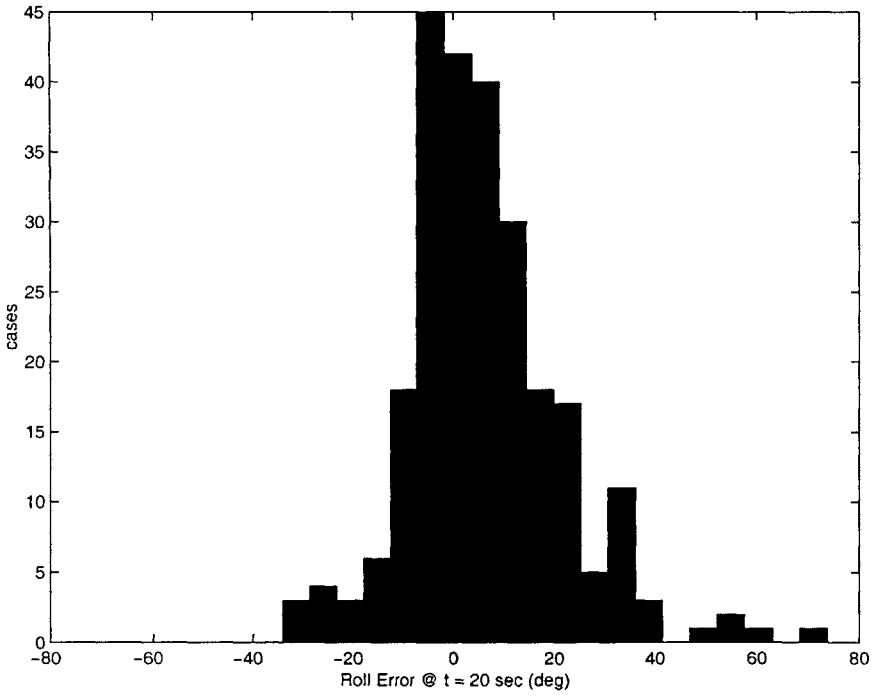


Figure 6-31: Roll angle estimation error distribution. ($\sigma_{rw} = 5$ milli-g/$\sqrt{\text{Hz}}$)

# Chapter 7

# Conclusions

## 7.1 Summary

This thesis has presented a dynamics-based algorithm for accelerometer-only navigation. The algorithm uses a 12-state extended Kalman filter for navigation, with additional states to model instrument biases. Additional navigation measurements are formulated based on the assumed dynamic properties of the projectile. The navigation algorithm was implemented in a 6-DOF simulation, and performance results for rate and attitude estimation presented. From the results of these tests, the following conclusions can be made:

- The navigation algorithm is very sensitive to errors in instrument orientation. Preliminary research at Draper has shown that sensor misalignments may be as large as 6 degrees. This figure must be substantially improved if accelerometer-only navigation is to succeed. Initial worst-case instrument error estimates made by Draper for several error sources are included in Table 7.1, along with a set of suggested minimum requirements based on the work in this thesis.

- The velocity alignment measurement formulation allows three axis attitude determination over time, based solely on assumptions about the vehicle dynamics. The quality of the measurement is dependent upon the amplitude of the angle of attack, as well as the quality of the firing solution.

- The digital IIR filter proposed to separate the secular pitch-over component of lateral rates does a good job of estimating roll attitude during flight. Formulation of the IIR filter output as a measurement in the main navigation filter also allows for a good estimate of roll error variance to be made in the navigation filter, as well as improving the instrument bias estimation performance of the filter.

- Rate estimation using accelerometers can be successful if the instruments are of sufficient quality, and if the roll rate of the platform is sufficiently large. However, problems arising from the non-linearity of the estimation algorithm require particular care if the navigation algorithm is to be successful. Unantici-

Table 7.1: Accelerometer error requirements and initial estimate

| Error Type | Draper Estimate | Required |
|---|---|---|
| $\sigma_{rw}$ (milli-g/$\sqrt{\text{Hz}}$) | 5 | 2.5 |
| Bias (milli-g) | 500 | 1000 |
| Misalignment Error (deg) | 6 | 1 |
| Scale Factor Error (ppm) | 1000 | 1000 |

pated errors encountered in real hardware could easily upset the careful balance achieved in simulation.

## 7.2 Suggestions for Further Research

Significant additional work remains before an accelerometer-only navigation system can be implemented in a real system. Several important issues encountered in the course of this thesis follow.

- In the navigation filter proposed, only bias errors are explicitly modelled. The potential use of additional error states, particularly misalignment and position error states, should be investigated.
- The effect of time-varying roll rate on rate estimation should be investigated. Rate estimation performance through roll rate sign transitions is of particular interest, since the filter presented here behaved poorly at very low constant rates.
- The effect of changing the accelerometer configuration, or increasing the number of accelerometers used, should be studied. Of particular interest are configurations that account for the difference in signal strength between lateral and roll components of angular rate.
- The sensitivity of the navigation algorithm to larger amplitude precession modes should be investigated. A larger mode would increase the error in the velocity alignment measurement proposed, and make it more difficult to isolate the pitch-over component of the lateral rate. The possibility of using additional states to represent the wind-relative angle of attack should be investigated. A possible method of doing this is presented in Appendix A.

# Appendix A

# Dynamics Model

This appendix presents a linearized aerodynamic model for an axially symmetric, spinning projectile taken from work by [2]. This model may be used to find an analytical expression for precession frequency useful in parameterizing the IIR filter as required in 6.2.2, or in estimating error characteristics for the vehicle alignment measurement defined in Section 5.2.

The simple velocity alignment assumption of Section 5.2 is sensitive to errors arising from non-zero vehicle angle of attack. A more sophisticated model that estimates this angle based on a model of the vehicle aerodynamic behavior might help to mitigate these errors. A possible method of doing this is presented in A.3. While this was method was not used in the final navigation filter presented in this thesis, it is of possible interest to future research.

## A.1 General Vehicle Dynamics

The vehicle dynamics can be modelled as a set of vector equations

$$\frac{d\boldsymbol{v}_B}{dt} + \boldsymbol{\omega}_B \times \boldsymbol{v}_B = \boldsymbol{s}_B + \boldsymbol{g}_B \tag{A.1}$$

$$\mathbf{I}\frac{d\boldsymbol{\omega}_B}{dt} + \boldsymbol{\omega}_B \times \mathbf{I}\boldsymbol{\omega}_B = \boldsymbol{m}_B \tag{A.2}$$

where $\boldsymbol{s}_B$ and $\boldsymbol{g}_B$ are the aerodynamic and gravitational accelerations, $\mathbf{I}$ is the moment of inertia, and $\boldsymbol{m}_B$ is the aerodynamic moment. The vehicle is assumed symmetric about the spin axis, so that

$$\mathbf{I} = \begin{bmatrix} I_X & 0 & 0 \\ 0 & I_T & 0 \\ 0 & 0 & I_T \end{bmatrix} \tag{A.3}$$

Defining the ratio of inertia tensor components $\mu = I_X/I_T$, (A.1) can be written component-wise as

$$\frac{dv_x}{dt} + \omega_y v_z - \omega_z v_y = s_x + g_x \tag{A.4}$$

$$\frac{dv_y}{dt} - \omega_x v_z + \omega_z v_x = s_y + g_y \tag{A.5}$$

$$\frac{dv_z}{dt} + \omega_x v_y - \omega_y v_x = s_z + g_z \tag{A.6}$$

and

$$\frac{d\omega_x}{dt} = \frac{1}{I_X} m_x \tag{A.7}$$

$$\frac{d\omega_y}{dt} - (1-\mu)\omega_x\omega_z = \frac{1}{I_X} m_x \tag{A.8}$$

$$\frac{d\omega_z}{dt} + (1-\mu)\omega_x\omega_y = \frac{1}{I_X} m_x \tag{A.9}$$

Defining new complex quantities in terms of the lateral velocity and rate components

$$z = v_y + iv_z \tag{A.10}$$

$$w = \omega_y + i\omega_z \tag{A.11}$$

and defining similar complex quantities for gravity $g_T = g_y + ig_z$, moment $m_t = m_y + im_z$, and acceleration $s_T = s_y + is_z$, the lateral component pairs of the dynamic equations can be reduced to

$$\frac{dz}{dt} + i\omega_x z - iwv_x = s_T + g_T \tag{A.12}$$

$$\frac{dw}{dt} + i\omega_c w = \frac{1}{I_T} m_T \tag{A.13}$$

where $\omega_c = (1-\mu)\omega_x$. The second equation can be transformed to an angle of attack representation by defining the complex angle of attack

$$u = \frac{v_y + iv_z}{v_x} \tag{A.14}$$

which changes the dynamic equations to

$$\frac{du}{dt} + i\omega_x u - iw = \frac{1}{v_x}(s_T + g_T) \tag{A.15}$$

$$\frac{dw}{dt} + i\omega_c w = \frac{1}{I_T} m_T \tag{A.16}$$

## A.2 Linearized Aerodynamics Model

For a given complex angle of attack, the forces and moments can be modelled as

$$s_T = -\frac{1}{M} C_{N_\alpha} A_{\text{ref}} q_\infty u \tag{A.17}$$

$$m_T = C_{M_\alpha} A_{\text{ref}} L_{\text{ref}} q_\infty iu + C_{M_q} \frac{1}{2V_\infty} A_{\text{ref}} L_{\text{ref}} D_{\text{ref}} q_\infty w \tag{A.18}$$

Using these expressions for the aerodynamic forces, equations (A.15) and (A.16) can be written as a coupled pair of linear equations with time-varying coefficients

$$\frac{du}{dt} = -K_F(t)u + iw + \frac{1}{v_x}g_T \tag{A.19}$$

$$\frac{dw}{dt} = iK_P(t)u - K_Q(t)w \tag{A.20}$$

where the coefficients are defined as

$$K_F(t) = \frac{1}{Mv_x}C_{N_\alpha}A_{\text{ref}}q_\infty + i\omega_x \tag{A.21}$$

$$K_P(t) = \frac{1}{I_T}C_{M_\alpha}A_{\text{ref}}L_{\text{ref}}q_\infty \tag{A.22}$$

$$K_Q(t) = i\omega_c - \frac{1}{I_T}C_{M_q}\frac{1}{2V_\infty}A_{\text{ref}}L_{\text{ref}}D_{\text{ref}}q_\infty \tag{A.23}$$

or in matrix form as

$$\frac{d}{dt}\begin{bmatrix} u \\ w \end{bmatrix} = \begin{bmatrix} -K_F & i \\ iK_P & -K_Q \end{bmatrix}\begin{bmatrix} u \\ w \end{bmatrix} + \frac{1}{v_x}\begin{bmatrix} g_T \\ 0 \end{bmatrix} \tag{A.24}$$

## A.3 Estimating Velocity Vector Misalignment

Assuming no wind, the complex angle of attack variable $\alpha$ can be rewritten as a small rotation from the vehicle nose to the body-frame velocity $\boldsymbol{v}_B$. Defining a small rotation vector $\boldsymbol{\varphi}_B$, such that

$$\boldsymbol{\varphi}_B = \begin{bmatrix} 0 \\ -\mathcal{I}(u) \\ \mathcal{R}(u) \end{bmatrix} \tag{A.25}$$

The linearized dynamics dictate that, for small angles

$$\frac{\boldsymbol{v}_b}{|\boldsymbol{v}_b|} = (\mathbf{I} + [\boldsymbol{\varphi}_B\times])\boldsymbol{i}_x \tag{A.26}$$

which, to first order, is just a restatement of the definition of $u$.

### State Equation for $\boldsymbol{\varphi}$

The transverse components of (A.26) can also be handled as a complex quantity $\varphi_T = \varphi_y + i\varphi_z$, such that $u = -i\varphi_T$. Using this definition, the first equation of (A.24) becomes

$$-i\frac{d\varphi_T}{dt} = -iK_F\varphi_T + iw + \frac{1}{v_x}g_T \tag{A.27}$$

$$\frac{d\varphi_T}{dt} = K_F\varphi_T - w + \frac{i}{v_x}g_T \tag{A.28}$$

Separation of real and imaginary components then gives an equation for $\boldsymbol{\varphi}_B$ in matrix form:

$$\frac{d\boldsymbol{\varphi}_B}{dt} = \begin{bmatrix} 0 & 0 & 0 \\ 0 & +\mathcal{R}(K_F) & -\mathcal{I}(K_F) \\ 0 & +\mathcal{I}(K_F) & +\mathcal{R}(K_F) \end{bmatrix} \boldsymbol{\varphi}_B - \begin{bmatrix} 0 & 0 & 0 \\ 0 & 1 & 0 \\ 0 & 0 & 1 \end{bmatrix} \boldsymbol{\omega}_B + \frac{1}{v_x} \begin{bmatrix} 0 & 0 & 0 \\ 0 & 0 & -1 \\ 0 & 1 & 0 \end{bmatrix} \begin{bmatrix} g_x \\ g_y \\ g_z \end{bmatrix} \tag{A.29}$$

Taking the gravity term in inertial coordinates, and noting that the $x$ component of velocity in the body frame $v_x \approx |\boldsymbol{v}_I|$,

$$\frac{d\boldsymbol{\varphi}_B}{dt} = \mathbf{K}\boldsymbol{\varphi}_B - \mathbf{I}_t\boldsymbol{\omega}_B + \frac{1}{|\boldsymbol{v}_I|}\mathbf{I}_g\mathbf{A}_{IB}^T\boldsymbol{g}_I \tag{A.30}$$

Rewriting in terms of the reference velocity alignment vector $\bar{\boldsymbol{\varphi}}_B$

$$\boldsymbol{\varphi}_B = \bar{\boldsymbol{\varphi}}_B + \delta\boldsymbol{\varphi}_B \tag{A.31}$$

The differential equation (A.30) can be written in terms of the perturbation state

$$\frac{d(\bar{\boldsymbol{\varphi}}_B + \delta\boldsymbol{\varphi}_B)}{dt} = \mathbf{K}\boldsymbol{\varphi}_B - \mathbf{I}_t\boldsymbol{\omega}_B + \frac{1}{|\boldsymbol{v}_I|}\mathbf{I}_g\mathbf{A}_{IB}^T g_I \tag{A.32}$$

Expanding,

$$\frac{d\bar{\boldsymbol{\varphi}}_B}{dt} + \frac{d(\delta\boldsymbol{\varphi}_B)}{dt} = \mathbf{K}(\bar{\boldsymbol{\varphi}}_B + \delta\boldsymbol{\varphi}_B) - \mathbf{I}_t(\bar{\boldsymbol{\omega}}_B + \delta\boldsymbol{\omega}_B) + \frac{1}{|\boldsymbol{v}_I|}\mathbf{I}_g(\mathbf{I} - [\boldsymbol{\psi}\times])\bar{\mathbf{A}}_{IB}^{\mathrm{T}}\boldsymbol{g}_I \tag{A.33}$$

and eliminating $\boldsymbol{\varphi}_B$,

$$\frac{d(\delta\boldsymbol{\varphi}_B)}{dt} = K\delta\boldsymbol{\varphi}_B - \mathbf{I}_t\delta\boldsymbol{\omega}_B + \frac{1}{|\boldsymbol{v}_I|}\mathbf{I}_g[(\bar{\mathbf{A}}_{IB}^{\mathrm{T}}\boldsymbol{g}_I)\times]\boldsymbol{\psi} \tag{A.34}$$

gives the differential equation for the velocity alignment in terms of previously defined filter states.

### Improved Velocity Misalignment Measurement

Returning to the relationship in (A.26), the velocity misalignment error equation of (5.12) can be more accurately described by incorporating the velocity off-pointing term. It is important to note here that although the rotation $\boldsymbol{\varphi}_B$ is represented as a 3 component vector, the first component has no physical significance. Taking the velocity misalignment in body coordinates, (5.12) can be written as

$$\boldsymbol{z}_{v_{mis}} = (\mathbf{I} - [\bar{\boldsymbol{\varphi}}_B\times])\bar{\mathbf{A}}_{IB}^{\mathrm{T}}\boldsymbol{i}_v - \boldsymbol{i}_x \tag{A.35}$$

The components of the partials matrix (5.16) must then be revised to include the angle of attack term. Expanding (A.35), and taking care not to allow perturbations in the first part of $\delta\boldsymbol{\varphi}_B$:

$$\boldsymbol{z}_{v_{mis}} = (\mathbf{I} - [(\boldsymbol{\varphi}_B - \mathbf{I}_t\delta\boldsymbol{\varphi}_B)\times])(\mathbf{I} + [\boldsymbol{\psi}\times])\mathbf{A}_{IB}^{\mathrm{T}}\boldsymbol{i}_v - \boldsymbol{i}_x \tag{A.36}$$

multiplying through, and taking only first order terms:

$$\boldsymbol{z}_{v_{mis}} = \{\mathbf{I} - [\boldsymbol{\varphi}\times] + [(\mathbf{I}_t\delta\boldsymbol{\varphi})\times] + (\mathbf{I} - [\boldsymbol{\varphi}\times])[\boldsymbol{\psi}\times]\}\mathbf{A}_{IB}^{\mathrm{T}}\boldsymbol{i}_v - \boldsymbol{i}_x \tag{A.37}$$

taking partials with respect to $\boldsymbol{\psi}_B$ and $\delta\boldsymbol{\varphi}_B$:

$$\mathbf{C}_{mis,\psi} \equiv \frac{\partial \boldsymbol{z}_{mis}}{\partial \boldsymbol{\psi}_B} = -(\mathbf{I} - [\boldsymbol{\varphi}\times])[(\mathbf{A}_{IB}^{\mathrm{T}}\boldsymbol{i}_v)\times] \tag{A.38}$$

$$\mathbf{C}_{mis,\varphi} \equiv \frac{\partial \boldsymbol{z}_{mis}}{\partial(\delta\boldsymbol{\varphi}_B)} = -[(\mathbf{A}_{IB}^{\mathrm{T}}\boldsymbol{i}_v)\times]\mathbf{I}_t \tag{A.39}$$

The measurement model can now be written in terms of the filter states, expanded to include the new alignment term:

$$\hat{\boldsymbol{z}}_{mis} = \begin{bmatrix} 0 & 0 & \mathbf{C}_{mis,\psi} & 0 & \mathbf{C}_{mis,\varphi} & 0 \end{bmatrix} \begin{bmatrix} \delta\boldsymbol{r}_I \\ \delta\boldsymbol{v}_I \\ \boldsymbol{\psi}_B \\ \delta\boldsymbol{\omega}_B \\ \delta\boldsymbol{\varphi}_B \\ \delta\boldsymbol{\beta} \end{bmatrix} + \boldsymbol{\nu}_{mis} \tag{A.40}$$

# References


[1] Asher, M., "Accelerometer-Only Inertial Navigation," Tech. Rep. PSF-93-153, APL, Dec. 1993.

[2] Bottkol, M., Personal Communications, March 2001.

[3] Brown, R. G. and Hwang, P. Y., *Introduction to Random Signals and Applied Kalman Filtering*, John Wiley & Sons, New York, 1997, pp. 181–204.

[4] Dowdle, J., Thorvaldsen, T., and Kourepenis, A., "A GPS/INS Guidance System for Navy 5" Projectile," *AIAA Guidance Navigation and Control Conference*, New Orleans, LA, Aug. 1997.

[5] Gustafson, D., Hopkins, R., Barbour, N., and Dowdle, J., "A Micromechanical INS/GPS System for Guided Projectiles," *Proc. 51$^{st}$ Annual Meeting of the Institute of Navigation*, Colorado Springs, CO, June 1995.

[6] Gustafson, D. and Lucia, D., "Autonomous Local Vertical Determination for Guided Artillery Shells," *Proc. 52$^{nd}$ Annual Meeting of the Institute of Navigation*, Cambridge, MA, June 1996.

[7] Kalman, R., "A New Approach to Linear Filtering and Prediction Problems," *Journal of Basic Engineering, Transactions of the American Society of Mechanical Engineers*, Vol. 82D, March 1960, pp. 35–45.

[8] Lucia, D., *Estimation of the Local Vertical State for a Guided Munition Shell with an Embedded GPS/Micro-Mechanical Inertial Navigation System*, Master's thesis, MIT, May 1995.

[9] Sitomer, J., Connelly, J., and Kourepenis, A., "Micromechanical Inertial Guidance, Navigation and Control Systems in Gun Launched Projectiles," *AIAA Journal of Guidance, Control, and Dynamics*, Portland, OR, Aug. 1999.

[10] Wertz, J. R., editor, *Spacecraft Attitude Determination and Control*, Kluwer Academic Publishers, Dordrecht, Holland, 1978, pp. 758–759.